

Intrinsic Thermal Hall Effect in Mott Insulators

Jixun K. Ding,^{1,2,*} Emily Z. Zhang,^{3,*} Wen O. Wang,^{1,2} Tessa Cookmeyer,⁴
Brian Moritz,¹ Yong Baek Kim,^{3,†} and Thomas P. Devereaux^{1,5,‡}

¹Stanford Institute for Materials and Energy Sciences,

SLAC National Accelerator Laboratory, 2575 Sand Hill Road, Menlo Park, CA 94025, USA

²Department of Applied Physics, Stanford University, Stanford, CA 94305, USA

³Department of Physics, University of Toronto, Toronto, Ontario M5S 1A7, Canada

⁴Kavli Institute for Theoretical Physics, University of California, Santa Barbara, CA 93106, USA

⁵Department of Materials Science and Engineering, Stanford University, Stanford, CA 94305, USA

(Dated: June 26, 2025)

In light of recent experimental data indicating a substantial thermal Hall effect in square lattice antiferromagnetic Mott insulators, we investigate whether a simple Mott insulator can sustain a finite thermal Hall effect. We verify that the answer is “no” if one performs calculations within a spin-only low-energy effective spin model with non-interacting magnons. However, by performing determinant quantum Monte Carlo simulations, we show the single-band t - t' - U Hubbard model coupled to an orbital magnetic field does support a finite thermal Hall effect when $t' \neq 0$ and $B \neq 0$ in the Mott insulating phase. We argue that the (carrier agnostic) necessary conditions for observing a finite thermal Hall effect are time-reversal and particle-hole symmetry breaking. By considering magnon-magnon scattering using a semi-classical Boltzmann analysis, we illustrate a physical mechanism by which finite transverse thermal conductivity may arise, consistent with our symmetry argument and numerical results. Our results contradict the conventional wisdom that square and triangular lattices with $SU(2)$ symmetry do not support a finite thermal Hall effect and call for a critical re-examination of thermal Hall effect data in insulating magnets, as the magnon contribution should not be excluded *a priori*.

Introduction.— Thermal Hall transport is a powerful experimental probe for diagnosing the underlying excitations in quantum materials. At its core, transverse heat transport is sensitive to the nontrivial topology of the heat carriers, and the mechanism by which the carriers acquire this topology depends on the nature of the excitation. This sensitivity is particularly advantageous in insulators where conventional charge transport experiments cannot be performed, allowing for the detection of charge neutral excitations, such as magnetic fluctuations (magnons) [1], lattice vibrations (phonons) [2, 3], and spin fractionalization (spinons) [4]. Understanding the unique signatures stemming from various quasiparticle excitations and the interplay between them continues to be a persistent pursuit within the field.

Recently, a large, negative thermal Hall conductivity κ_{xy} was measured in the undoped Mott insulating phase of various cuprate superconductors [5–7], as well as the antiferromagnetic insulator Cu_3TeO_6 [8]. While the large signal observed down to low temperatures has mainly been attributed to phonons, the exact mechanism by which the phonons acquire chirality remains under debate [9–14]. This uncertainty leads us to consider other charge-neutral excitations that yield a finite thermal Hall signal.

A sizable κ_{xy} can also arise from topological magnon excitations of magnetically ordered states [1, 15–18]. The magnons may generically acquire a nontrivial topology due to exchange interactions that break global spin rotation ($SU(2)$) symmetry, such as the bond-dependent Kitaev interaction on honeycomb lattices [19, 20], or the antisymmetric Dzyaloshinskii-Moriya (DM) interac-

tion [21, 22], leading to finite transverse thermal transport. In the case where $SU(2)$ symmetry is preserved, e.g. with Heisenberg-type Hamiltonians with a ring exchange, certain lattice geometries are believed to be barred from exhibiting a thermal Hall effect due to various no-go theorems [4]. The antiferromagnetic order on the square lattice seen in cuprate insulators is an example of one of these forbidden geometries. These no-go theorems, however, were derived using non-interacting magnons within the context of linear spin-wave theory (LSWT). While it has been postulated that κ_{xy} should still be negligible when perturbing away from this limit (e.g. via a small canting of the spin moments) [23], the effects of incorporating magnon-magnon interactions are unknown, but can in principle contribute to the thermal Hall effect [24–27]. Moreover, for insulating phases close to the Mott transition, enhanced charge fluctuations leading to higher-order exchange terms may arise in the spin Hamiltonian, whose inclusion may also contribute to thermal Hall transport. Calculating the magnon thermal Hall coefficient including these effects without using simplifying assumptions or perturbative approaches is theoretically challenging, even on the simple square lattice. In an effort to overcome this hurdle, we raise a more fundamental question: Without assuming a particular magnon model, what are the requirements for observing a finite thermal Hall effect in Mott insulators?

In this paper, we study the t - t' - U Hubbard-Hofstadter model on the square lattice, which captures essential features of high- T_c cuprates under a magnetic field. We emphasize that this model does not include extrinsic

sources of scattering, such as phonons and disorder, so any mechanism for finite transport are intrinsic to the model electronic Hamiltonian. First, we examine the symmetry requirements for a finite thermal Hall response to exist. While our model does not break spin SU(2) symmetry, the applied orbital magnetic field breaks time-reversal symmetry (TRS), and the inclusion of second nearest-neighbor hopping t' breaks particle-hole symmetry (PHS). We demonstrate that one cannot obtain a finite thermal Hall conductivity in particle-hole symmetric systems, even if TRS is broken. Heuristically, we then expect that in systems without PHS, the thermal Hall conductivity is generically nonzero. We use determinant Quantum Monte Carlo (DQMC) [28, 29] to compute κ_{xy} in the undoped Mott insulating phase, and explicitly demonstrate the relationship between PHS breaking and nonzero κ_{xy} . By increasing $|t'|$, which controls the degree of PHS breaking, we observe an increase in the thermal Hall conductivity. We find that the computed κ_{xy}/T is on the order of 0.01 to 0.1 k_B^2/\hbar at $T/t = 1/5$, $B = 0.0625\Phi_0/a^2$, where $\Phi_0 = hc/e$ is the magnetic flux quantum and a is the lattice constant.

Finally, we consider magnon-magnon scattering as one possible mechanism for generating a finite thermal Hall effect using the semiclassical theory of Ref. [27]. Projecting into the low-energy spin Hamiltonian results in an effective J_1 - J_2 - J_χ model, in which the chiral J_χ term only appears when both t' and B are present. Using a semi-classical Boltzmann analysis, we demonstrate that only the collision processes mediated by the J_χ interaction contribute to the transverse thermal conductivity, consistent with both our symmetry argument and our numerical results. Our findings illustrate the limitations of linear spin wave theory, and imply that intrinsic spin fluctuations should not be excluded as transverse heat carriers *a priori* when interpreting thermal Hall experiments in insulating magnets.

Model and Numerical Methods.— We study the single-band Hubbard-Hofstadter model

$$H = - \sum_{ij\sigma} t_{ij} \left\{ \exp[i\varphi_{ij}] c_{i\sigma}^\dagger c_{j\sigma} + \text{h.c.} \right\} - \mu \sum_{i\sigma} n_{i\sigma} + U \sum_i (n_{i\uparrow} - 1/2)(n_{i\downarrow} - 1/2), \quad (1)$$

on a two-dimensional square lattice at half-filling. The hopping integral $t_{ij} = t$ between nearest neighbor sites $\langle ij \rangle$, $t_{ij} = t'$ between next-nearest neighbor sites $\langle\langle ij \rangle\rangle$, and $t_{ij} = 0$ otherwise. μ is the chemical potential, and U is the on-site Coulomb interaction strength. $c_{i\sigma}^\dagger$ ($c_{i\sigma}$) is the creation (annihilation) operator for an electron on site i with spin $\sigma = \uparrow, \downarrow$ and $n_{i\sigma} = c_{i\sigma}^\dagger c_{i\sigma}$ measures the number of electrons of spin σ on site i . A spatially uniform and static orbital magnetic field is introduced by

Peierls substitution via the phase

$$\varphi_{ij} = \frac{2\pi}{\Phi_0} \int_{\mathbf{r}_i}^{\mathbf{r}_j} \mathbf{A} \cdot d\boldsymbol{\ell}, \quad (2)$$

where $\mathbf{r}_i = (r_{ix}, r_{iy})$ is the position of site i , and the path integral is taken along the shortest straight line path between sites i and j . The vector potential \mathbf{A} generates the out-of-plane magnetic field $\mathbf{B} = B\hat{\mathbf{z}}$. In this work we use the symmetric gauge $\mathbf{A}(\mathbf{r}) = B(-r_y\hat{\mathbf{x}} + r_x\hat{\mathbf{y}})/2$.

DQMC simulations of Eq. (1) are performed on a finite cluster with lattice constant $a = 1$, and $N_x = 8$ and $N_y = 8$ sites in the $\hat{\mathbf{x}}$ and $\hat{\mathbf{y}}$ directions, respectively. We implement modified periodic boundary conditions [30], described in detail elsewhere [31]. Requiring that the wave function be single-valued on the torus gives the flux quantization condition $\Phi/\Phi_0 = N_\phi/N$, where $N = N_x N_y$ denotes the total number of sites, $\Phi = Ba^2$ is the magnetic flux threading each unit cell, and N_ϕ is an integer. Detailed DQMC simulation parameters are listed in Supplementary Materials (SM) [32], Section S1.

Within DQMC simulations, we measure unequal imaginary time electric/heat current - electric/heat current correlation functions, which are related to frequency-resolved transport coefficients via the Kubo formulas [33]. DQMC measures

$$\chi_{\mu\nu,\alpha\beta}(\tau) = \frac{1}{V} \langle J_{\mu,\alpha}(\tau) J_{\nu,\beta}(0) \rangle, \quad (3)$$

where τ is imaginary time, μ, ν index current type 1, 2 representing charge and heat current respectively, and α, β index directions x, y . When $\mu = \nu$ and $\alpha = \beta$, MaxEnt analytic continuation [34] is used to convert correlators in imaginary time, Eq. (3), to retarded correlators in real frequency, $\chi_{\mu\nu,\alpha\beta}(\omega)$, which is proportional to the conductivity. However, when $\mu = \nu$ and $\alpha \neq \beta$, the off-diagonal correlator $\chi_{\mu\mu,xy}(\omega)$ need not be positive over all frequencies, which precludes us from directly applying the standard MaxEnt algorithm [35–37]. This is a known issue for off-diagonal spectral functions, and in this work, we adopt two different methods to circumvent this difficulty and estimate the thermal Hall response: 1) a subtraction method suggested by Ref. [35, 36], involving performing analytic continuation on a composite object, then subtracting off the diagonal component; and 2) a finite-Matsubara-frequency proxy proposed in our earlier work [38], involving estimating the Hall coefficient with its value at the first nonzero Matsubara frequency. We demonstrate that these two methods give qualitatively similar results. A detailed description of these two approaches can be found in SM [32], Section S4.

Symmetry Argument.— Here, we outline a simple derivation demonstrating that the thermal Hall coefficient is symmetry enforced to be strictly zero when the Hamiltonian respects chiral symmetry (i.e. when $t' = 0$ in the square lattice case), even when a nonzero magnetic field breaks TRS.

Consider the unitary charge conjugation transform \mathcal{C} , which acts as $c_{i\sigma} \rightarrow (-1)^i c_{i\sigma}^\dagger$, $c_{i\sigma}^\dagger \rightarrow (-1)^i c_{i\sigma}$, where $(-1)^i$ depends on the sublattice [39]. Also consider the anti-unitary time-reversal transformation \mathcal{T} , which acts as $i \rightarrow -i$. The combination $\mathcal{C} \cdot \mathcal{T}$ is the anti-unitary chiral symmetry, \mathcal{S} [40]. In the presence of a magnetic field, the Hamiltonian Eq. (1) with $t'/t = 0$ on a square lattice at half-filling breaks \mathcal{C} and \mathcal{T} individually, but satisfies the combined \mathcal{S} symmetry. Considering the \mathcal{C} transformation alone, the Hamiltonian transforms as

$$H(\mathbf{A}) \rightarrow \mathcal{C}H(\mathbf{A})\mathcal{C}^{-1} = H(-\mathbf{A}) \quad (4)$$

while the heat current operator \mathbf{J}_Q transforms as

$$\mathbf{J}_Q(\mathbf{A}) \rightarrow \mathcal{C}\mathbf{J}_Q(\mathbf{A})\mathcal{C}^{-1} = \mathbf{J}_Q(-\mathbf{A}). \quad (5)$$

As a result, the transverse current-current correlator in imaginary time, $\chi_{22,xy} = \frac{1}{V} \langle J_{Q,x}(\mathbf{A}, \tau) J_{Q,y}(\mathbf{A}) \rangle$, and therefore κ_{xy} , satisfy

$$\chi_{22,xy}(\mathbf{A}) = \chi_{22,xy}(-\mathbf{A}) \quad (6)$$

$$\kappa_{xy}(\mathbf{A}) = \kappa_{xy}(-\mathbf{A}). \quad (7)$$

However, the transport response coefficients must also obey the Onsager-Casimir relation $\kappa_{xy}(\mathbf{A}) = \kappa_{yx}(-\mathbf{A})$, thus enforcing $\kappa_{xy}(\mathbf{A}) = \kappa_{xy}(-\mathbf{A}) = 0$. The same proof also applies to the electrical Hall and Seebeck coefficients, as shown in the SM [32], Section S6.

On the other hand, when $t' \neq 0$, Eqs. (4) and (5) are no longer satisfied, so the thermal Hall conductivity is symmetry-allowed to be nonzero. Indeed, our numerical findings in the following section not only demonstrate this effect, but that $|t'|$, which controls the degree of PHS breaking, also dictates the magnitude of κ_{xy} .

Results.— In Fig. 1, we show representative temperature dependence of longitudinal frequency-dependent electrical and thermal conductivities for Hubbard interaction strength $U/t = 6$, obtained by DQMC simulations. As temperature is lowered, the electrical conductivity becomes gapped, while the thermal conductivity exhibits a drude-like peak near $\omega = 0$. This phenomenology is consistent with prior work [41, 42], and tells us that below temperature scale $T \sim J \sim 4t^2/U$, charge degrees of freedom are frozen out, and magnons are the dominant heat carriers in the system. The behavior shown in Fig. 1 is representative in the sense that it does not depend on different next-nearest neighbor hopping t'/t and field strength B , as shown in the SM [32], Figure S6.

To further examine the divergent behavior of charge and heat transport, in Fig. 2 we show the DC ($\omega \rightarrow 0$) conductivities, charge compressibility χ_c , specific heat c_V , and electrical and thermal diffusivities D and D^Q , extracted using

$$D = \frac{\sigma}{\chi_c}, \quad D^Q = \frac{\kappa}{c_V}. \quad (8)$$

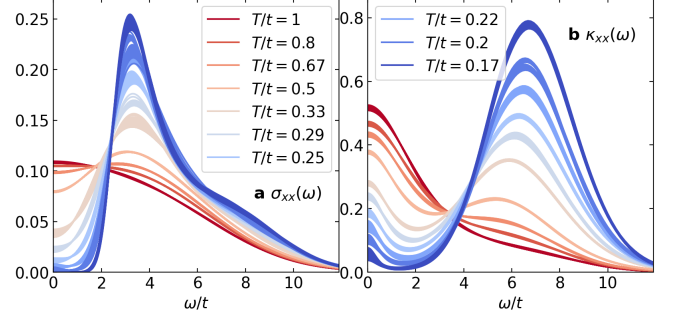


FIG. 1. Temperature dependence of longitudinal frequency-dependent **a** electrical conductivity $\sigma_{xx}(\omega)$, and **b** thermal conductivity $\kappa_{xx}(\omega)$, for the Hubbard-Hofstadter model with $U/t = 6$, $t'/t = -0.1$, at half-filling $\langle n \rangle = 1$ and fixed field strength $\Phi/\Phi_0 = 4/64$. 100 bootstrap resamples are shown. Both panels share the same legend.

By comparing Fig. 2e-f, we see that at the lowest temperatures we access, the charge diffusivity approaches zero while the thermal diffusivity exhibits an upturn. This further confirms that at $T/t \lesssim 0.2$, we are dealing with an electrical insulator and thermal conductor, with the longitudinal thermal conduction well-understood in terms of magnons [42].

Next, we use two different methods (see SM [32], Section S4) to obtain the DC thermal Hall conductivity κ_{xy}^{DC} , thermal Hall angle $\theta_{\text{th,H}}$, and thermal Hall coefficient $R_{\text{th,H}}$, and show the results in Fig. 3. The two methods produce qualitatively similar results: while the thermal Hall response is zero at all temperatures when $t' = 0$ (within error bars), the thermal Hall response is generically positive and nonzero, with a magnitude that increases with increasing $|t'|$. The high-temperature behavior may be attributed to thermally excited hole-like charge carriers inherited from the underlying tight-binding band structure, which orbitally couple to the magnetic field. However, the low temperature ($T \lesssim J$) thermal Hall response, which we have argued is due to heat transport by magnons, evidently violates the no-go result [4]. We have verified setting Hubbard interaction $U/t = 8$ produces qualitatively similar results as the $U/t = 6$ case shown here, and finite-size effects are minimal (see SM [32] for additional plots). These checks give us confidence that the observed nonzero thermal Hall effect at low temperatures are neither remnant signatures of charge fluctuations nor finite-size artifacts.

Discussion.— How do we reconcile the apparent contradiction between our numerical results in Fig. 3 and the no-go result [4]? A careful reading reveals that the no-go result is a restricted statement about linear spin-wave theory, which does not account for effects due to magnon-magnon scattering.

Performing a strong-coupling expansion on the Hubbard-Hofstadter model shows that the low-energy

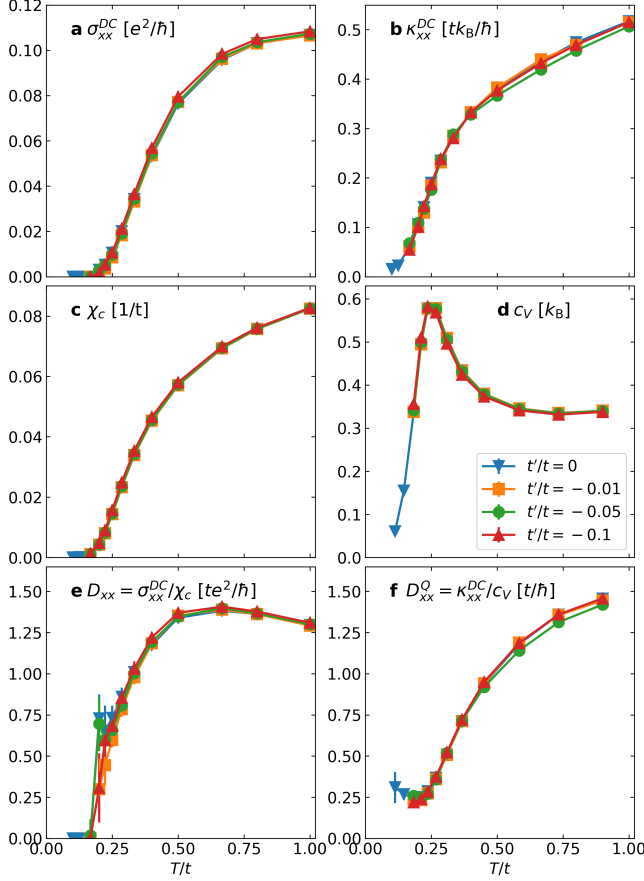


FIG. 2. **a** Longitudinal DC electrical conductivity σ_{xx}^{DC} , **b** longitudinal DC thermal conductivity κ_{xx}^{DC} , **c** charge compressibility χ_c , **d** specific heat c_V , **e** charge diffusivity D_{xx} , and **f** thermal diffusivity D_{xx}^Q in the Hubbard-Hofstadter model with $U/t = 6$ at half-filling $\langle n \rangle = 1$ and magnetic field strength $\Phi/\Phi_0 = 4/64$. All panels share the same legend.

effective spin Hamiltonian to order $\mathcal{O}(t^3/U^2)$ includes a scalar spin chirality term [43, 44]

$$H_{\text{eff}} = J_1 \sum_{\langle ij \rangle} \mathbf{S}_i \cdot \mathbf{S}_j + J_2 \sum_{\langle\langle ij \rangle\rangle} \mathbf{S}_i \cdot \mathbf{S}_j + J_\chi \sum_{\triangle_{ijk}} \mathbf{S}_i \cdot (\mathbf{S}_j \times \mathbf{S}_k), \quad (9)$$

where

$$J_1 = \frac{4t^2}{U}, \quad J_2 = \frac{4t'^2}{U}, \quad J_\chi = \frac{24t^2t'}{U^2} \sin(\pi\Phi/\Phi_0), \quad (10)$$

and \triangle_{ijk} denotes a triangular plaquette with lattice sites i, j, k in anticlockwise order. At the quadratic level, J_χ does not endow the magnon bands with nontrivial Berry curvature required for thermal Hall transport [16], as it vanishes both in linear spin-wave theory [4] and at the mean-field level [32]. However, it was recently discovered that magnon-magnon scattering, which does not depend on topological band theory, may give rise to a finite thermal Hall coefficient [27].

As a minimal example, we illustrate this mechanism using semi-classical Boltzmann transport, in which the

thermal Hall conductivity is related to the rate of magnon mode collisions (or collision kernel) by [27]

$$\kappa_{xy} = \frac{1}{2k_B T^2 V} \sum_{\mathbf{k}, \mathbf{k}'} (\mathbf{v}_{\mathbf{k}} \times \mathbf{v}_{\mathbf{k}'})_z \varepsilon_{\mathbf{k}} \varepsilon_{\mathbf{k}'} \tau_{\mathbf{k}} \tau_{\mathbf{k}'} G_{\mathbf{k}} G_{\mathbf{k}'} \mathcal{A}_{\mathbf{k}\mathbf{k}'}, \quad (11)$$

where $\varepsilon_{\mathbf{k}}$ is the dispersion, $\mathbf{v}_{\mathbf{k}} = \partial \varepsilon_{\mathbf{k}} / \partial \mathbf{k}$ is the magnon group velocity, $\tau_{\mathbf{k}}$ is the magnon lifetime, and $G_{\mathbf{k}} = \sqrt{\bar{N}_{\mathbf{k}}(\bar{N}_{\mathbf{k}} + 1)}$, where $\bar{N}_{\mathbf{k}}$ is the Bose-Einstein distribution. Here, $\mathcal{A}_{\mathbf{k}\mathbf{k}'} = (\mathcal{O}_{\mathbf{k}\mathbf{k}'} - \mathcal{O}_{\mathbf{k}'\mathbf{k}})/2$ is the antisymmetric part of the collision kernel, where $\mathcal{O}_{\mathbf{k}\mathbf{k}'}$ is the total off-diagonal scattering rate, composed of $\mathcal{O}_{\mathbf{k}\mathbf{k}'}^{++}$, $\mathcal{O}_{\mathbf{k}\mathbf{k}'}^{--}$, $\mathcal{O}_{\mathbf{k}\mathbf{k}'}^{+-}$, and $\mathcal{O}_{\mathbf{k}\mathbf{k}'}^{-+}$. The \pm superscripts describe scattering events where modes with the corresponding momentum subscripts are created (+) or destroyed (-). These scattering rates may be computed using Fermi's Golden Rule [27].

It can be shown that in order for $\mathcal{A}_{\mathbf{k}\mathbf{k}'}$, and therefore κ_{xy} , to be finite, the microscopic detailed balance relations

$$\frac{\mathcal{O}_{\mathbf{k}\mathbf{k}'}^{++}}{\mathcal{O}_{\mathbf{k}\mathbf{k}'}^{--}} = e^{-\beta \varepsilon_{\mathbf{k}'}} \quad \frac{\mathcal{O}_{\mathbf{k}\mathbf{k}'}^{+-}}{\mathcal{O}_{\mathbf{k}\mathbf{k}'}^{-+}} = e^{\beta \varepsilon_{\mathbf{k}'}} \quad (12)$$

must be violated [13, 27, 45]. If we consider the J_1 - J_2 - J_χ model, we find that only the collisions mediated by the J_χ term violate Eq. (12). In other words, one cannot generate a finite κ_{xy} from magnon-magnon scattering without both $t' \neq 0$ and $\Phi \neq 0$ on the square lattice, which is consistent with our numerical results and symmetry argument. Moreover, the leading order contribution is an interference process between a first and second order scattering event, implying $\kappa_{xy} \propto J_\chi J_1^2 \sim t' \sin(\pi\Phi/\Phi_0)$. The linear magnetic field dependence (when $\Phi \ll \Phi_0$) and linear t' dependence of κ_{xy} are consistent with our numerical results, as shown in SM [32], Figure S11, and Fig. 3, respectively.

We emphasize that the magnon-magnon scattering picture from the downfolded spin-Hamiltonian is only one mechanism for generating a finite thermal Hall. In contrast, our DQMC results are valid independently of any specific thermal current carriers or the assumptions of Boltzmann scattering, and is a more general demonstration of the violation of the no-go theorem.

While it is tempting to directly compare the magnitude of the thermal Hall conductivity κ_{xy}/T we obtain to experimental values [5], we emphasize that when converted to units appropriate to cuprate materials, e.g. $t/k_B \sim 4000\text{K}$ and $a = 3.8\text{\AA}$, our lowest temperature corresponds to $T \sim 700\text{K}$, and our lowest magnetic field strength corresponds to $B \sim 400\text{T}$. It is not at all straightforward to extrapolate our results to experimentally reasonable temperatures $T \lesssim 100\text{K}$ and field strengths $B \sim 10\text{T}$, so we won't attempt to do so. The main focus of this work is a demonstration of the intrinsic mechanism of the thermal Hall effect, rather than a quantitative prediction of the thermal Hall signal in the cuprates. Our

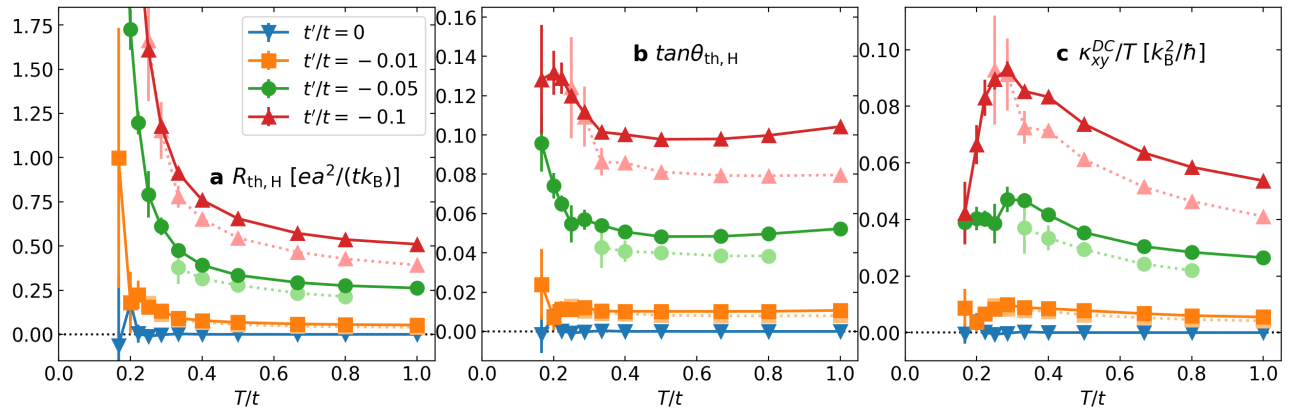


FIG. 3. **a** DC thermal Hall coefficient, **b** thermal Hall angle, and **c** thermal Hall conductivity. Solid lines denote results obtained by the proxy method, while dotted lines denote results obtained by the subtraction method (See SM [32] for detailed methods). Hubbard $U/t = 6$ and field strength $\Phi/\Phi_0 = 4/64$. All panels share the same legend.

work primarily serves as a “proof of principle”: we establish that the t - t' - U Hubbard model on the square lattice exhibits a nonzero thermal Hall effect under an applied magnetic field. Therefore, in analyzing experimental data, one should not naively ignore potential magnon contributions to the thermal Hall effect based on the no-go theorem [4], which has a much narrower regime of validity than commonly interpreted.

Data Availability.— Aggregated numerical data and analysis routines required to reproduce the figures can be found at [10.5281/zenodo.13799597](https://zenodo.org/record/13799597). Raw simulation data that support the findings of this study are stored on the Sherlock cluster at Stanford University and are available from the corresponding author upon reasonable request.

Code Availability.— The most up-to-date version of our thermal transport DQMC simulation code can be accessed at <https://github.com/katherineding/dqmc-dev>.

Acknowledgements.— We are grateful for helpful discussions with Steve Kivelson, Alexander Balatsky, Anjishnu Bose, Junkai Dong, Nishchhal Verma, Vladimir Calvera, Alexander Mook, and Julian May-Mann.

This work was supported by the U.S. Department of Energy (DOE), Office of Basic Energy Sciences, Division of Materials Sciences and Engineering. Computational work was performed on the Sherlock cluster at Stanford University and on resources of the National Energy Research Scientific Computing Center (NERSC), a Department of Energy Office of Science User Facility, using NERSC award BES-ERCAP0027200. E.Z.Z. and Y.B.K. are supported by the Natural Science and Engineering Research Council (NSERC) of Canada and the Center for Quantum Materials at the University of Toronto. E.Z.Z. was further supported by the Michael Smith Foreign Study Scholarship. T.C. is supported by a University of California Presidential Postdoctoral Fellowship and acknowledges support from the Gordon and Betty Moore Foundation

through Grant No. GBMF8690 to UC Santa Barbara.

* These authors contributed equally to this work

† yongbaek.kim@utoronto.ca

‡ tpd@stanford.edu

- [1] P. A. McClarty, Topological magnons: A review, *Annual Review of Condensed Matter Physics* **13**, 171 (2022).
- [2] T. Qin, J. Zhou, and J. Shi, Berry curvature and the phonon Hall effect, *Phys. Rev. B* **86**, 104305 (2012).
- [3] T. Saito, K. Misaki, H. Ishizuka, and N. Nagaosa, Berry Phase of Phonons and Thermal Hall Effect in Nonmagnetic Insulators, *Physical Review Letters* **123**, 255901 (2019).
- [4] H. Katsura, N. Nagaosa, and P. A. Lee, Theory of the thermal Hall effect in quantum magnets, *Phys. Rev. Lett.* **104**, 066403 (2010).
- [5] G. Grissonnanche, A. Legros, S. Badoux, E. Lefrançois, V. Zlatko, M. Lizaire, F. Laliberté, A. Gourgout, J.-S. Zhou, S. Pyon, T. Takayama, H. Takagi, S. Ono, N. Doiron-Leyraud, and L. Taillefer, Giant thermal Hall conductivity in the pseudogap phase of cuprate superconductors, *Nature* **571**, 376 (2019).
- [6] G. Grissonnanche, S. Thériault, A. Gourgout, M.-E. Boulanger, E. Lefrançois, A. Ataei, F. Laliberté, M. Dion, J.-S. Zhou, S. Pyon, T. Takayama, H. Takagi, N. Doiron-Leyraud, and L. Taillefer, Chiral phonons in the pseudogap phase of cuprates, *Nature Physics* **16**, 1108 (2020).
- [7] M.-E. Boulanger, G. Grissonnanche, S. Badoux, A. Al-laire, É. Lefrançois, A. Legros, A. Gourgout, M. Dion, C. H. Wang, X. H. Chen, R. Liang, W. N. Hardy, D. A. Bonn, and L. Taillefer, Thermal Hall conductivity in the cuprate Mott insulators Nd_2CuO_4 and $\text{Sr}_2\text{CuO}_2\text{Cl}_2$, *Nature Communications* **11**, 5325 (2020).
- [8] L. Chen, M.-E. Boulanger, Z.-C. Wang, F. Tafti, and L. Taillefer, Large phonon thermal Hall conductivity in the antiferromagnetic insulator Cu_3TeO_6 , *Proceedings of the National Academy of Sciences* **119**, e2208016119 (2022).
- [9] X.-Q. Sun, J.-Y. Chen, and S. A. Kivelson, Large extrin-

- sis phonon thermal Hall effect from resonant scattering, *Physical Review B* **106**, 144111 (2022).
- [10] B. Flebus and A. H. MacDonald, Charged defects and phonon Hall effects in ionic crystals, *Phys. Rev. B* **105**, L220301 (2022).
 - [11] M. Ye, L. Savary, and L. Balents, Phonon Hall viscosity in magnetic insulators (2021), [arXiv:2103.04223 \[cond-mat.str-el\]](#).
 - [12] H. Guo, D. G. Joshi, and S. Sachdev, Resonant thermal Hall effect of phonons coupled to dynamical defects, *Proceedings of the National Academy of Sciences* **119**, e2215141119 (2022).
 - [13] L. Mangeolle, L. Balents, and L. Savary, Phonon thermal Hall conductivity from scattering with collective fluctuations, *Physical Review X* **12**, 041031 (2022).
 - [14] T. Oh and N. Nagaosa, Phonon thermal hall effect in mott insulators via skew-scattering by the scalar spin chirality (2024), [arXiv:2408.01671 \[cond-mat.str-el\]](#).
 - [15] Y. Onose, T. Ideue, H. Katsura, Y. Shiomi, N. Nagaosa, and Y. Tokura, Observation of the magnon Hall effect, *Science* **329**, 297 (2010).
 - [16] R. Matsumoto, R. Shindou, and S. Murakami, Thermal Hall effect of magnons in magnets with dipolar interaction, *Physical Review B* **89**, 054420 (2014).
 - [17] S. Murakami and A. Okamoto, Thermal Hall Effect of Magnons, *Journal of the Physical Society of Japan* **86**, 011010 (2017).
 - [18] X.-T. Zhang, Y. H. Gao, and G. Chen, Thermal Hall effects in quantum magnets, *Physics Reports* **1070**, 1 (2024).
 - [19] P. A. McClarty, X.-Y. Dong, M. Gohlke, J. G. Rau, F. Pollmann, R. Moessner, and K. Penc, Topological magnons in Kitaev magnets at high fields, *Physical Review B* **98**, 060404 (2018).
 - [20] E. Z. Zhang, L. E. Chern, and Y. B. Kim, Topological magnons for thermal Hall transport in frustrated magnets with bond-dependent interactions, *Physical Review B* **103**, 174402 (2021).
 - [21] H. Doki, M. Akazawa, H.-Y. Lee, J. H. Han, K. Sugii, M. Shimozaawa, N. Kawashima, M. Oda, H. Yoshida, and M. Yamashita, Spin thermal Hall conductivity of a kagome antiferromagnet, *Phys. Rev. Lett.* **121**, 097203 (2018).
 - [22] P. Laurell and G. A. Fiete, Magnon thermal hall effect in kagome antiferromagnets with dzyaloshinskii-moriya interactions, *Phys. Rev. B* **98**, 094419 (2018).
 - [23] R. Samajdar, S. Chatterjee, S. Sachdev, and M. S. Scheurer, Thermal hall effect in square-lattice spin liquids: A schwinger boson mean-field study, *Phys. Rev. B* **99**, 165126 (2019).
 - [24] C. Carnahan, Y. Zhang, and D. Xiao, Thermal Hall effect of chiral spin fluctuations, *Physical Review B* **103**, 224419 (2021).
 - [25] A. Mook, K. Plekhanov, J. Klinovaja, and D. Loss, Interaction-stabilized topological magnon insulator in ferromagnets, *Phys. Rev. X* **11**, 021061 (2021).
 - [26] A. Mook, R. Hoyer, J. Klinovaja, and D. Loss, Magnons, magnon bound pairs, and their hybrid spin-multipolar topology, *Phys. Rev. B* **107**, 064429 (2023).
 - [27] D. Chatzichrysafis and A. Mook, Thermal Hall Effect of Magnons from Many-Body Skew Scattering (2024), [2407.00423 \[cond-mat\]](#).
 - [28] S. R. White, D. J. Scalapino, R. L. Sugar, E. Y. Loh, J. E. Gubernatis, and R. T. Scalettar, Numerical study of the two-dimensional Hubbard model, *Physical Review B* **40**, 506 (1989).
 - [29] E. Y. Loh, J. E. Gubernatis, R. T. Scalettar, S. R. White, D. J. Scalapino, and R. L. Sugar, Sign problem in the numerical simulation of many-electron systems, *Physical Review B* **41**, 9301 (1990).
 - [30] F. F. Assaad, Depleted Kondo lattices: Quantum Monte Carlo and mean-field calculations, *Phys. Rev. B* **65**, 115104 (2002).
 - [31] J. K. Ding, L. Yang, W. O. Wang, Z. Zhu, C. Peng, P. Mai, E. W. Huang, B. Moritz, P. W. Phillips, B. E. Feldman, and T. P. Devereaux, Particle-hole asymmetric ferromagnetism and spin textures in the triangular Hubbard-Hofstadter model (2024), [arXiv:2309.07876 \[cond-mat.str-el\]](#).
 - [32] See Supplemental Material [url insterted by publisher] for details on the numerical methods, symmetry argument, magnon-magnon analysis, mean-field analysis, comments on the energy magnetization term, and supplementary plots, which includes Refs. [46–54].
 - [33] B. S. Shastry, Electrothermal transport coefficients at finite frequencies, *Reports on Progress in Physics* **72**, 016501 (2008).
 - [34] M. Jarrell and J. Gubernatis, Bayesian inference and the analytic continuation of imaginary-time quantum Monte Carlo data, *Physics Reports* **269**, 133 (1996).
 - [35] A. Reymbaut, D. Bergeron, and A.-M. S. Tremblay, Maximum Entropy Analytic Continuation for Spectral Functions with Non-Positive Spectral Weight, *Physical Review B* **92**, 060509 (2015), [arxiv:1507.01956 \[cond-mat\]](#).
 - [36] A. Reymbaut, A.-M. Gagnon, D. Bergeron, and A.-M. S. Tremblay, Maximum entropy analytic continuation for frequency-dependent transport coefficients with nonpositive spectral weight, *Physical Review B* **95**, 121104 (2017).
 - [37] J. Fei, C.-N. Yeh, D. Zgid, and E. Gull, Analytical continuation of matrix-valued functions: Carathéodory formalism, *Physical Review B* **104**, 165111 (2021).
 - [38] W. O. Wang, J. K. Ding, B. Moritz, Y. Schattner, E. W. Huang, and T. P. Devereaux, Numerical approaches for calculating the low-field DC Hall coefficient of the doped Hubbard model, *Phys. Rev. Research* **3**, 033033 (2021).
 - [39] This is usually called a particle-hole transformation for the Hubbard model at zero applied magnetic field.
 - [40] C.-K. Chiu, J. C. Y. Teo, A. P. Schnyder, and S. Ryu, Classification of topological quantum matter with symmetries, *Reviews of Modern Physics* **88**, 035005 (2016).
 - [41] E. W. Huang, R. Sheppard, B. Moritz, and T. P. Devereaux, Strange metallicity in the doped Hubbard model, *Science* **366**, 987 (2019).
 - [42] W. O. Wang, J. K. Ding, B. Moritz, E. W. Huang, and T. P. Devereaux, Magnon heat transport in a two-dimensional Mott insulator, *Phys. Rev. B* **105**, L161103 (2022).
 - [43] D. Sen and R. Chitra, Large- u limit of a Hubbard model in a magnetic field: Chiral spin interactions and paramagnetism, *Physical Review B* **51**, 1922 (1995).
 - [44] O. I. Motrunich, Orbital magnetic field effects in spin liquid with spinon Fermi sea: Possible application to κ -(ET)₂Cu₂(CN)₃, *Physical Review B* **73**, 155115 (2006).
 - [45] L. Mangeolle, L. Balents, and L. Savary, Thermal conductivity and theory of inelastic scattering of phonons by collective fluctuations, *Phys. Rev. B* **106**, 245139 (2022).
 - [46] D. Bergeron and A.-M. S. Tremblay, Algorithms for optimized maximum entropy and diagnostic tools for analytic continuation, *Phys. Rev. E* **94**, 023303 (2016).

- [47] G. Mahan, *Many-Particle Physics*, Physics of Solids and Liquids (Springer US, 2013).
- [48] M. Marder, *Condensed Matter Physics* (Wiley, 2010).
- [49] J. M. Luttinger, Theory of Thermal Transport Coefficients, *Physical Review* **135**, A1505 (1964).
- [50] M. Rigol and B. S. Shastry, Drude weight in systems with open boundary conditions, *Physical Review B* **77**, 161101 (2008), [arxiv:0801.0592 \[cond-mat\]](#).
- [51] F. F. Assaad and M. Imada, Hall coefficient for the two-dimensional Hubbard model, *Physical Review Letters* **74**, 3868 (1995).
- [52] T. Qin, Q. Niu, and J. Shi, Energy magnetization and the thermal Hall effect, *Physical Review Letters* **107**, 236601 (2011).
- [53] J. H. Han and H. Lee, Spin chirality and Hall-like transport phenomena of spin excitations, *Journal of the Physical Society of Japan* **86**, 011007 (2017).
- [54] H. B. Callen, The Application of Onsager's Reciprocal Relations to Thermoelectric, Thermomagnetic, and Galvanomagnetic Effects, *Physical Review* **73**, 1349 (1948).

Supplementary Material to “Intrinsic Thermal Hall Effect in Mott Insulators”

S1 Simulation Parameters

Determinant quantum Monte Carlo (DQMC) data shown in main text figures are obtained from simulations performed using 2×10^4 to 5×10^4 warm-up sweeps and 3×10^5 to 5×10^6 measurement sweeps through the auxillary field. We run 120 to 500 independently seeded Markov chains for each set of parameters. For all parameter values, the imaginary time discretization interval $\Delta\tau \leq 0.05/t$, and the number of imaginary time slices $L = \beta/\Delta\tau \geq 10$. Such a small imaginary time discretization interval is chosen in order to reduce effects from Trotter error. The chemical potential is fine tuned so that particle density satisfies $|\langle n \rangle - 1| < 4 \times 10^{-5}$, as shown in Fig. S1.

In all simulations, multiple equal-time measurements are taken in each full measurement sweep through the auxillary field, while unequal-time measurements are taken every few full measurement sweeps. Specifically, each Markov chain with M measurement sweeps collects $ML/5$ equal-time measurements, and $M/2$ unequal-time measurements. The mean and standard error of equal-time observables and the finite-Matsubara-frequency proxy are estimated via jackknife resampling of independent Markov chains. The mean and standard error of MaxEnt results are estimated via bootstrap resampling of independent Markov chains using 100 bootstrap samples. In MaxEnt fits, we always use flat model functions and choose hyper-parameter α using the “BT” method [1]. For the subtraction method described in Section S4.1, the same bootstrap resamples are used for both the composite object and the longitudinal response.

S2 Electrical Current Operator

Charge current is carried by particle current: $\mathbf{J} = (-e)\mathbf{J}_N$. The particle current operator is easy to find, e.g. see ref. [2], where we define a polarization operator $\mathbf{P} = \sum_j \mathbf{R}_j n_j$ and find $\mathbf{J}_N = \frac{i}{\hbar}[H, \mathbf{P}]$. Written out explicitly, the total charge current operator is

$$\mathbf{J} = \frac{i(-e)}{\hbar} \sum_{ij\sigma} t_{ij} \exp[i\varphi_{ij}] (\mathbf{R}_i - \mathbf{R}_j) c_{i\sigma}^\dagger c_{j\sigma} \quad (1)$$

$$= \frac{ie}{2\hbar} \sum_{ij\sigma} t_{ij} (\mathbf{R}_j - \mathbf{R}_i) \left[\exp[i\varphi_{ij}] c_{i\sigma}^\dagger c_{j\sigma} - \exp[i\varphi_{ji}] c_{j\sigma}^\dagger c_{i\sigma} \right], \quad (2)$$

which componentwise becomes

$$J_x = \frac{i(-e)}{\hbar} \sum_{ij\sigma} t_{ij} \exp[i\varphi_{ij}] c_{i\sigma}^\dagger c_{j\sigma} (x_i - x_j), \quad (3)$$

$$J_y = \frac{i(-e)}{\hbar} \sum_{ij\sigma} t_{ij} \exp[i\varphi_{ij}] c_{i\sigma}^\dagger c_{j\sigma} (y_i - y_j). \quad (4)$$

Current operators are Hermitian, even in presence of nonzero magnetic field. So we can always write

$$J_x^\dagger = J_x, \quad J_y^\dagger = J_y. \quad (5)$$

S3 Heat Current Operator

Energy currents flow whenever heat is generated or dissipated *non-uniformly* in the solid. (Total) energy current \mathbf{J}_E has units [energy · velocity] and obeys continuity equation [2] (Here H should not include the chemical potential term):

$$\frac{\partial}{\partial t} H + \nabla \cdot \mathbf{J}_E = 0.$$

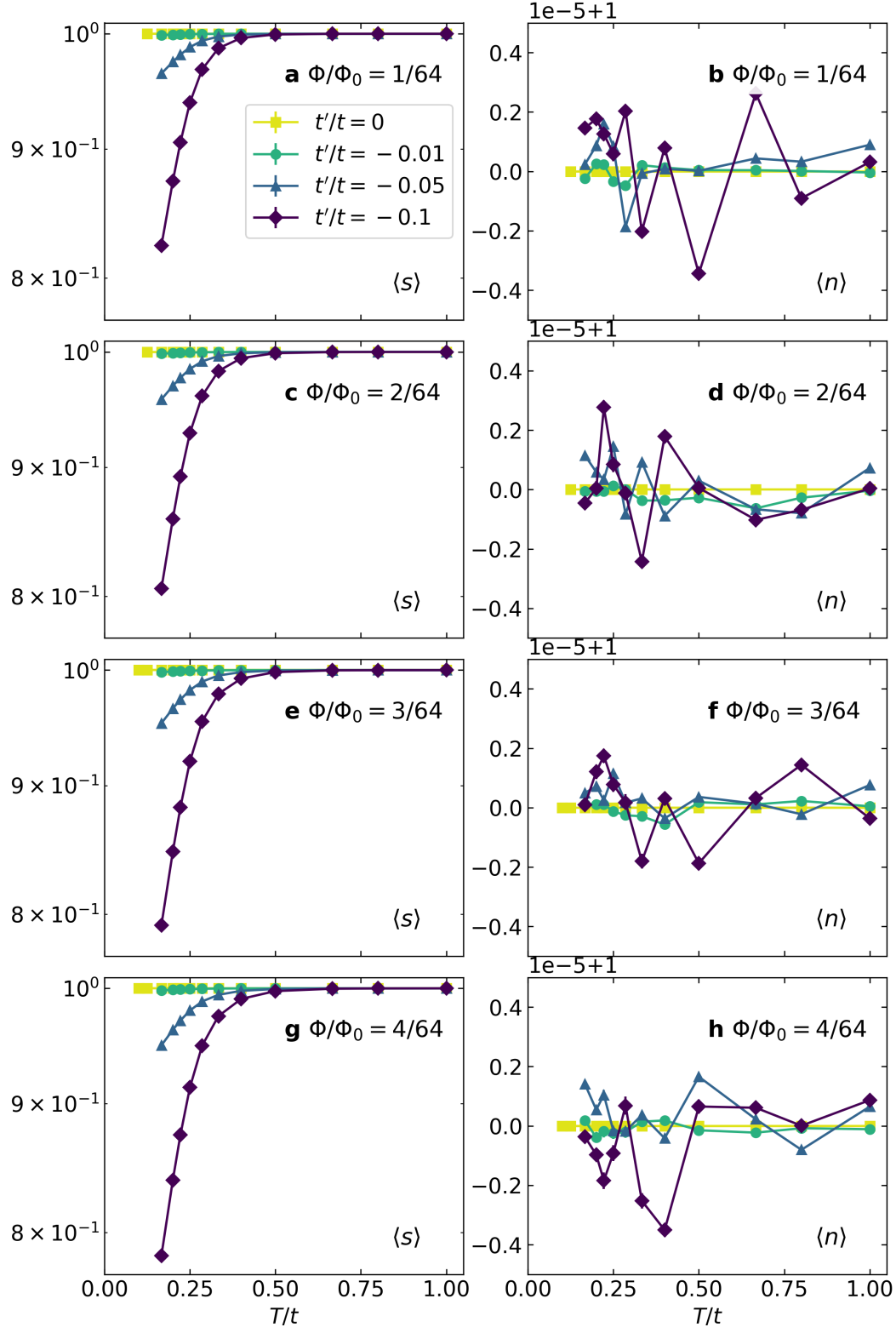


Figure S1: Fermion sign and average particle density after chemical potential tuning. Hubbard $U/t = 6$, target half filling $\langle n \rangle = 1$. Errorbars (smaller than the size of the data points) denote one standard deviation of the mean, determined by jackknife resampling.

Completely analogous to how we defined a polarization operator to find the expression for the particle current operator, we formally introduce an operator \mathbf{R}_E ,

$$\mathbf{R}_E = \frac{1}{2} \int d\mathbf{r} [\mathbf{r} \mathcal{H}(\mathbf{r}) + \mathcal{H}(\mathbf{r}) \mathbf{r}], \quad (6)$$

where $\mathcal{H}(\mathbf{r})$ is the hamiltonian/energy density, which allows us to find the energy current via

$$\frac{d\mathbf{R}_E}{dt} = \frac{i}{\hbar} [H, \mathbf{R}_E] = \mathbf{J}_E. \quad (7)$$

What is \mathbf{R}_E in the Hubbard model? Using

$$H = - \sum_{ij\sigma} t_{ij} \exp[\varphi_{ij}] c_{i\sigma}^\dagger c_{j\sigma} + U \sum_i \left(c_{i\uparrow}^\dagger c_{i\uparrow} - 1/2 \right) \left(c_{i\downarrow}^\dagger c_{i\downarrow} - 1/2 \right), \quad (8)$$

$$h_i = -\frac{1}{2} \sum_{j\sigma} t_{ij} \left(\exp[\varphi_{ij}] c_{i\sigma}^\dagger c_{j\sigma} + \exp[\varphi_{ji}] c_{j\sigma}^\dagger c_{i\sigma} \right) + U \left(c_{i\uparrow}^\dagger c_{i\uparrow} - \frac{1}{2} \right) \left(c_{i\downarrow}^\dagger c_{i\downarrow} - \frac{1}{2} \right), \quad (9)$$

we find

$$\mathbf{R}_E = \sum_i \mathbf{R}_i h_i = -\frac{1}{2} \sum_{ij\sigma} \mathbf{R}_i t_{ij} \left(\exp[\varphi_{ij}] c_{i\sigma}^\dagger c_{j\sigma} + \exp[\varphi_{ji}] c_{j\sigma}^\dagger c_{i\sigma} \right) + U \sum_i \mathbf{R}_i \left(c_{i\uparrow}^\dagger c_{i\uparrow} - \frac{1}{2} \right) \left(c_{i\downarrow}^\dagger c_{i\downarrow} - \frac{1}{2} \right). \quad (10)$$

Note that we wrote h_i in the form Eq. (9) because we desire that it be explicitly hermitian $h_i = h_i^\dagger$. Using the above allows us to get \mathbf{J}_E :

$$\begin{aligned} \mathbf{J}_E &= \frac{i}{\hbar} [H - \mu N, \mathbf{R}_E] = \\ &= \frac{i}{\hbar} \left[- \sum_{ij\sigma} t_{ij} \exp[\varphi_{ij}] c_{i\sigma}^\dagger c_{j\sigma} - \mu \sum_{i\sigma} c_{i\sigma}^\dagger c_{i\sigma} + U \sum_i \left(c_{i\uparrow}^\dagger c_{i\uparrow} - 1/2 \right) \left(c_{i\downarrow}^\dagger c_{i\downarrow} - 1/2 \right), \right. \\ &\quad \left. - \frac{1}{2} \sum_{ij\sigma} \mathbf{R}_i t_{ij} \left(\exp[\varphi_{ij}] c_{i\sigma}^\dagger c_{j\sigma} + \exp[\varphi_{ji}] c_{j\sigma}^\dagger c_{i\sigma} \right) + U \sum_i \mathbf{R}_i \left(c_{i\uparrow}^\dagger c_{i\uparrow} - \frac{1}{2} \right) \left(c_{i\downarrow}^\dagger c_{i\downarrow} - \frac{1}{2} \right) \right] \\ &= \frac{i}{\hbar} \left[- \sum_{ij\sigma} t_{ij} \exp[\varphi_{ij}] c_{i\sigma}^\dagger c_{j\sigma} - \left(\mu + \frac{1}{2} U \right) \sum_{i\sigma} n_{i\sigma} + U \sum_i n_{i\uparrow} n_{i\downarrow}, \right. \\ &\quad \left. - \frac{1}{2} \sum_{ij\sigma} \mathbf{R}_i t_{ij} \left(\exp[\varphi_{ij}] c_{i\sigma}^\dagger c_{j\sigma} + \exp[\varphi_{ji}] c_{j\sigma}^\dagger c_{i\sigma} \right) - \frac{1}{2} U \sum_{i\sigma} \mathbf{R}_i n_{i\sigma} + U \sum_i \mathbf{R}_i n_{i\uparrow} n_{i\downarrow} \right]. \quad (11) \end{aligned}$$

There are 3 terms in Hamiltonian, 3 terms in \mathbf{R}_E . We label the 3 terms in the Hamiltonian “K,” “N,” and “U,” and the 3 terms in \mathbf{R}_E “RK,” “RN,” and “RU.” The commutator has 9 terms in total; 4 of them involve only commutation between number operators (namely the “N”-“RN,” “N”-“RU,” “U”-“RN,” “U”-“RU” combinations) are identically zero. We compute the rest manually.

We make use of fermion commutator relations

$$[c_{i\sigma}^\dagger, n_{k\sigma'}] = -\delta_{ik} \delta_{\sigma\sigma'} c_{k\sigma'}^\dagger, \quad [c_{i\sigma}, n_{k\sigma'}] = \delta_{ik} \delta_{\sigma\sigma'} c_{k\sigma'},$$

and the following derived identities:

$$[c_{i\sigma}^\dagger c_{j\sigma}, n_{k\sigma'}] = \left(c_{i\sigma}^\dagger c_{k\sigma'} \delta_{jk} - c_{k\sigma'}^\dagger c_{j\sigma} \delta_{ik} \right) \delta_{\sigma\sigma'}, \quad (12)$$

$$[c_{i\sigma}^\dagger c_{j\sigma}, n_{k\uparrow} n_{k\downarrow}] = n_{k\downarrow} \delta_{\sigma\uparrow} \left(c_{i\sigma}^\dagger c_{k\uparrow} \delta_{jk} - c_{k\uparrow}^\dagger c_{j\sigma} \delta_{ik} \right) + n_{k\uparrow} \delta_{\sigma\downarrow} \left(c_{i\sigma}^\dagger c_{k\downarrow} \delta_{jk} - c_{k\downarrow}^\dagger c_{j\sigma} \delta_{ik} \right), \quad (13)$$

$$[c_{i\sigma}^\dagger c_{j\sigma}, c_{m\sigma'}^\dagger c_{n\sigma'}] = \left(c_{i\sigma}^\dagger c_{n\sigma'} \delta_{mj} - c_{m\sigma'}^\dagger c_{j\sigma} \delta_{ni} \right) \delta_{\sigma\sigma'}. \quad (14)$$

Eq. (12) tells us that the “N”-“RK” cross term is

$$\left[\left(\mu + \frac{1}{2}U \right) \sum_{k\sigma'} n_{k\sigma'}, -\frac{1}{2} \sum_{ij\sigma} \mathbf{R}_i t_{ij} \left(\exp[\varphi_{ij}] c_{i\sigma}^\dagger c_{j\sigma} + \exp[\varphi_{ji}] c_{j\sigma}^\dagger c_{i\sigma} \right) \right] = 0, \quad (15)$$

and the “K”-“RN” cross term is

$$\left[-\sum_{ij\sigma} t_{ij} \exp[\varphi_{ij}] c_{i\sigma}^\dagger c_{j\sigma}, -\frac{1}{2}U \sum_{k\sigma} \mathbf{R}_k n_{k\sigma} \right] = \frac{1}{2}U \sum_{ij\sigma} t_{ij} \exp[i\varphi_{ij}] (\mathbf{R}_j - \mathbf{R}_i) c_{i\sigma}^\dagger c_{j\sigma}. \quad (16)$$

The “K”-“RU” and “U”-“RK” kinetic-double occupancy cross terms are a little more involved. We compute using Eq. (13)

$$\begin{aligned} & \left[-\sum_{ij\sigma} t_{ij} \exp[\varphi_{ij}] c_{i\sigma}^\dagger c_{j\sigma}, U \sum_k \mathbf{R}_k n_{k\uparrow} n_{k\downarrow} \right] + \left[U \sum_k n_{k\uparrow} n_{k\downarrow}, -\frac{1}{2} \sum_{ij\sigma} \mathbf{R}_i t_{ij} \left(\exp[\varphi_{ij}] c_{i\sigma}^\dagger c_{j\sigma} + \exp[\varphi_{ji}] c_{j\sigma}^\dagger c_{i\sigma} \right) \right] \\ &= -U \sum_{ijk\sigma} t_{ij} \exp[i\varphi_{ij}] \mathbf{R}_k \left[c_{i\sigma}^\dagger c_{j\sigma}, n_{k\uparrow} n_{k\downarrow} \right] - \frac{1}{2}U \sum_{ijk\sigma} t_{ij} \exp[i\varphi_{ij}] (\mathbf{R}_i + \mathbf{R}_j) \left[n_{k\uparrow} n_{k\downarrow}, c_{i\sigma}^\dagger c_{j\sigma} \right] \\ &= -U \sum_{ijk\sigma} t_{ij} \exp[i\varphi_{ij}] \left[\mathbf{R}_k - \frac{1}{2} (\mathbf{R}_i + \mathbf{R}_j) \right] \left[c_{i\sigma}^\dagger c_{j\sigma}, n_{k\uparrow} n_{k\downarrow} \right] \\ &= -\frac{1}{2}U \sum_{ij} t_{ij} \exp[i\varphi_{ij}] (\mathbf{R}_j - \mathbf{R}_i) [(n_{i\downarrow} + n_{j\downarrow}) c_{i\uparrow} c_{j\uparrow} + (n_{i\uparrow} + n_{j\uparrow}) c_{i\downarrow} c_{j\downarrow}] \\ &= -\frac{1}{2}U \sum_{ij\sigma} t_{ij} \exp[i\varphi_{ij}] (\mathbf{R}_j - \mathbf{R}_i) (n_{i\sigma} + n_{j\sigma}) c_{i\bar{\sigma}}^\dagger c_{j\bar{\sigma}}. \end{aligned}$$

Finally, there is the “K”-“RK” term. Using Eq. (14) we have:

$$\begin{aligned} & \left[-\sum_{ij\sigma} t_{ij} \exp[i\varphi_{ij}] c_{i\sigma}^\dagger c_{j\sigma}, -\sum_{mn\sigma'} \mathbf{R}_m t_{mn} \exp[i\varphi_{mn}] c_{m\sigma}^\dagger c_{n\sigma} \right] \\ &= \sum_{ijmn\sigma} t_{ij} \exp[i\varphi_{ij}] \mathbf{R}_m t_{mn} \exp[i\varphi_{mn}] \left(c_{i\sigma}^\dagger c_{n\sigma} \delta_{mj} - c_{m\sigma}^\dagger c_{j\sigma} \delta_{ni} \right) \\ &= \sum_{ijn\sigma} t_{ij} \exp[i\varphi_{ij}] \mathbf{R}_j t_{jn} \exp[i\varphi_{jn}] c_{i\sigma}^\dagger c_{n\sigma} - \sum_{ijm\sigma} t_{ij} \exp[i\varphi_{ij}] \mathbf{R}_m t_{mi} \exp[i\varphi_{mi}] c_{m\sigma}^\dagger c_{j\sigma} \\ &= \sum_{ijk\sigma} t_{ij} t_{jk} \exp[i\varphi_{ij}] \exp[i\varphi_{jk}] (\mathbf{R}_j - \mathbf{R}_i) c_{i\sigma}^\dagger c_{k\sigma}, \end{aligned} \quad (17)$$

and

$$\begin{aligned} & \left[-\sum_{ij\sigma} t_{ij} \exp[i\varphi_{ij}] c_{i\sigma}^\dagger c_{j\sigma}, -\sum_{mn\sigma'} \mathbf{R}_m t_{mn} \exp[i\varphi_{nm}] c_{n\sigma}^\dagger c_{m\sigma} \right] \\ &= \sum_{ijmn\sigma} t_{ij} \exp[i\varphi_{ij}] \mathbf{R}_m t_{mn} \exp[i\varphi_{nm}] \left(c_{i\sigma}^\dagger c_{m\sigma} \delta_{nj} - c_{n\sigma}^\dagger c_{j\sigma} \delta_{mi} \right) \\ &= \sum_{ijm\sigma} t_{ij} \exp[i\varphi_{ij}] \mathbf{R}_m t_{mj} \exp[i\varphi_{jm}] c_{i\sigma}^\dagger c_{m\sigma} - \sum_{ijn\sigma} t_{ij} \exp[i\varphi_{ij}] \mathbf{R}_i t_{in} \exp[i\varphi_{ni}] c_{n\sigma}^\dagger c_{j\sigma} \\ &= \sum_{ijk\sigma} t_{ij} t_{jk} \exp[i\varphi_{ij}] \exp[i\varphi_{jk}] (\mathbf{R}_k - \mathbf{R}_j) c_{i\sigma}^\dagger c_{k\sigma}. \end{aligned} \quad (18)$$

Putting Eqs. (17) and (18) together, we have

$$\begin{aligned} & \left[- \sum_{ij\sigma} t_{ij} \exp[\varphi_{ij}] c_{i\sigma}^\dagger c_{j\sigma}, - \frac{1}{2} \sum_{mn\sigma} \mathbf{R}_m t_{mn} (\exp[\varphi_{mn}] c_{m\sigma}^\dagger c_{n\sigma} + \exp[\varphi_{nm}] c_{n\sigma}^\dagger c_{m\sigma}) \right] \\ &= \frac{1}{2} \sum_{ijk\sigma} t_{ij} t_{jk} \exp[i\varphi_{ij}] \exp[i\varphi_{jk}] (\mathbf{R}_k - \mathbf{R}_i) c_{i\sigma}^\dagger c_{k\sigma}. \end{aligned}$$

Summing all terms together, we have

$$\begin{aligned} \mathbf{J}_E &= \frac{i}{\hbar} \left\{ \frac{1}{2} \sum_{ijk\sigma} t_{ij} t_{jk} \exp[i\varphi_{ij}] \exp[i\varphi_{jk}] (\mathbf{R}_k - \mathbf{R}_i) c_{i\sigma}^\dagger c_{k\sigma} \right. \\ &\quad - \frac{1}{2} U \sum_{ij\sigma} t_{ij} \exp[i\varphi_{ij}] (\mathbf{R}_j - \mathbf{R}_i) (n_{i\sigma} + n_{j\sigma}) c_{i\bar{\sigma}}^\dagger c_{j\bar{\sigma}} \\ &\quad \left. + \frac{1}{2} U \sum_{ij\sigma} t_{ij} \exp[i\varphi_{ij}] (\mathbf{R}_j - \mathbf{R}_i) c_{i\sigma}^\dagger c_{j\sigma} \right\} \\ &= \frac{i}{\hbar} \left\{ \frac{1}{4} \sum_{ijk\sigma} t_{ij} t_{jk} (\mathbf{R}_k - \mathbf{R}_i) \left[\exp[i\varphi_{ij}] \exp[i\varphi_{jk}] c_{i\sigma}^\dagger c_{k\sigma} - \exp[i\varphi_{ji}] \exp[i\varphi_{kj}] c_{k\sigma}^\dagger c_{i\sigma} \right] \right. \\ &\quad - \frac{1}{4} U \sum_{ij\sigma} t_{ij} (\mathbf{R}_j - \mathbf{R}_i) (n_{i\sigma} + n_{j\sigma}) \left[\exp[i\varphi_{ij}] c_{i\bar{\sigma}}^\dagger c_{j\bar{\sigma}} - \exp[i\varphi_{ji}] c_{j\bar{\sigma}}^\dagger c_{i\bar{\sigma}} \right] \\ &\quad \left. + \frac{1}{4} U \sum_{ij\sigma} t_{ij} (\mathbf{R}_j - \mathbf{R}_i) \left[\exp[i\varphi_{ij}] c_{i\sigma}^\dagger c_{j\sigma} - \exp[i\varphi_{ji}] c_{j\sigma}^\dagger c_{i\sigma} \right] \right\}. \end{aligned}$$

But energy current is not the current which describes thermal conductivity or thermoelectric power. The (total) heat current is defined using (total) energy current and (total) particle current as

$$\mathbf{J}_Q = \mathbf{J}_E - \mu \mathbf{J}_N.$$

Particle current \mathbf{J}_N is (see Section S2)

$$\begin{aligned} \mathbf{J}_N &= -\frac{i}{\hbar} \sum_{ij\sigma} t_{ij} \exp[i\varphi_{ij}] (\mathbf{R}_j - \mathbf{R}_i) c_{i\sigma}^\dagger c_{j\sigma} \\ &= -\frac{i}{2\hbar} \sum_{ij\sigma} t_{ij} (\mathbf{R}_j - \mathbf{R}_i) \left[\exp[i\varphi_{ij}] c_{i\sigma}^\dagger c_{j\sigma} - \exp[i\varphi_{ji}] c_{j\sigma}^\dagger c_{i\sigma} \right], \end{aligned}$$

so the heat current \mathbf{J}_Q is

$$\begin{aligned} \mathbf{J}_Q &= \frac{i}{\hbar} \left\{ \frac{1}{4} \sum_{ijk\sigma} t_{ij} t_{jk} (\mathbf{R}_k - \mathbf{R}_i) \left[\exp[i\varphi_{ij}] \exp[i\varphi_{jk}] c_{i\sigma}^\dagger c_{k\sigma} - \exp[i\varphi_{ji}] \exp[i\varphi_{kj}] c_{k\sigma}^\dagger c_{i\sigma} \right] \right. \\ &\quad - \frac{1}{4} U \sum_{ij\sigma} t_{ij} (\mathbf{R}_j - \mathbf{R}_i) (n_{i\sigma} + n_{j\sigma}) \left[\exp[i\varphi_{ij}] c_{i\bar{\sigma}}^\dagger c_{j\bar{\sigma}} - \exp[i\varphi_{ji}] c_{j\bar{\sigma}}^\dagger c_{i\bar{\sigma}} \right] \\ &\quad \left. + \frac{1}{4} (U + 2\mu) \sum_{ij\sigma} t_{ij} (\mathbf{R}_j - \mathbf{R}_i) \left[\exp[i\varphi_{ij}] c_{i\sigma}^\dagger c_{j\sigma} - \exp[i\varphi_{ji}] c_{j\sigma}^\dagger c_{i\sigma} \right] \right\}. \end{aligned} \quad (19)$$

Heat current operators are Hermitian, even in presence of nonzero magnetic field. So we can always write

$$J_{Q,x}^\dagger = J_{Q,x}, \quad J_{Q,y}^\dagger = J_{Q,y}. \quad (20)$$

S4 Detailed Methods

A description of linear response, Kubo formulas, transport theory can be found in standard textbooks [2, 3, 4], but it's important to keep the sign, normalization, and notational conventions consistent throughout, so we briefly describe this formalism below.

We first note that computing the response to a nonuniform temperature requires some care since the thermal gradient does not directly modify the Hamiltonian as a usual perturbation, but rather the Boltzmann factor $e^{-H/k_B T(\mathbf{r})}$. We follow the formalism introduced by Luttinger [5], where we consider an expansion to the temperature as $T(\mathbf{r}) = T(1 - \psi(\mathbf{r}))$, where $\psi(\mathbf{r})$ is a small deviation from T , and is also known as a pseudogravitational potential. Up to terms linear in ψ , the Boltzmann factor becomes

$$e^{-H/k_B T(\mathbf{r})} = e^{-H/k_B T(1-\psi(\mathbf{r}))} \simeq e^{-H(1+\psi)/k_B T}. \quad (21)$$

Considering the more general case of a time-dependent perturbation, we may now write $H = H_0 + F$, where

$$H_0 = \int d\mathbf{r} h_0(\mathbf{r}) \quad \text{and} \quad F = \int d\mathbf{r} \psi(\mathbf{r}, t) h_0(\mathbf{r}). \quad (22)$$

Next, we consider the thermal-electric linear response equations

$$\mathbf{j} = L^{(11)} \mathbf{E} + L^{(12)} [-\nabla \psi] \quad (23)$$

$$\mathbf{j}_Q = L^{(21)} \mathbf{E} + L^{(22)} [-\nabla \psi] \quad (24)$$

where \mathbf{j} is the electric current density, \mathbf{j}_Q is the heat current density, T is temperature, and \mathbf{E} is electric field.

Note each $L^{(\mu\nu)}$ is itself a matrix, which, for our two dimensional system, has x and y components. The coefficients $L_{\alpha\beta}^{(\mu\nu)}$ are generally complex numbers, where μ, ν index current type 1, 2 representing charge and heat current respectively, α, β index directions x, y , can be computed via Kubo formulas and expressed in terms of retarded current-current operators¹

$$L_{\alpha\beta}^{(\mu\nu)} = \frac{1}{\hbar\omega V} \int_{-\infty}^{\infty} dt \theta(t) \langle [J_{\mu,\alpha}^\dagger(t), J_{\nu,\beta}(0)] \rangle_0 e^{i\omega t} = \frac{i}{\omega} \chi_{\mu\nu,\alpha\beta}^R(\omega), \quad (25)$$

where the retarded correlators in real frequency and real time are

$$\chi_{\mu\nu,\alpha\beta}^R(\omega) = \frac{-i}{\hbar V} \int_{-\infty}^{\infty} dt \theta(t) \langle [J_{\mu,\alpha}^\dagger(t), J_{\nu,\beta}(0)] \rangle_0 e^{i\omega t} = \int_{-\infty}^{\infty} dt \chi_{\mu\nu,\alpha\beta}^R(t) e^{i\omega t}, \quad (26)$$

$$\chi_{\mu\nu,\alpha\beta}^R(t) = \frac{-i}{\hbar V} \theta(t) \langle [J_{\mu,\alpha}^\dagger(t), J_{\nu,\beta}(0)] \rangle_0 = \frac{1}{2\pi} \int_{-\infty}^{\infty} d\omega \chi_{\mu\nu,\alpha\beta}^R(\omega) e^{-i\omega t}, \quad (27)$$

and $\mathbf{J} = \mathbf{j}(\mathbf{q} = 0)$ is the total electrical current operator, $\mathbf{J}_Q = \mathbf{j}_q(\mathbf{q} = 0)$ is the total heat current operator. Operators evolve in time according to the interaction representation, $\langle \rangle_0$ denotes taking expectation value in the unperturbed thermodynamic ensemble, and $V = Na^2$ is system volume. Derivations and explicit forms of total current operators are shown in Sections S2 and S3.

As \mathbf{J} has units of eta/\hbar , $L^{(11)}$ and σ have units of e^2/\hbar , and R_H has units of a^2/e . As \mathbf{J}_Q has units of $t^2 a/\hbar$, $L^{(22)}$ has units of t^2/\hbar , κ has units of tk_B/\hbar , κ/T has units of k_B^2/\hbar , and $R_{th,H}$ has units of $ea^2/(tk_B)$.

The retarded current-current correlators defined in Eqs. (26) and (27) can be written in Lehmann/spectral form as

$$\chi_{\mu\nu,\alpha\beta}^R(\omega) = \frac{1}{ZV} \sum_{mn} \frac{e^{-\beta E_n} - e^{-\beta E_m}}{\omega\hbar + i\delta + E_n - E_m} \langle n | J_{\mu,\alpha} | m \rangle \langle m | J_{\nu,\beta} | n \rangle, \quad (28)$$

$$\chi_{\mu\nu,\alpha\beta}^R(t) = \frac{1}{ZV} \frac{-i}{\hbar} \theta(t) \sum_{nm} [e^{-\beta E_n} - e^{-\beta E_m}] \langle n | J_{\mu,\alpha} | m \rangle \langle m | J_{\nu,\beta} | n \rangle e^{i(E_n - E_m)t/\hbar}, \quad (29)$$

where Z is the partition function, and E_n and E_m denote the eigenvalues of the Hamiltonian.

By writing $\chi_{\mu\nu,\alpha\beta}^R(\omega) = \chi_{\mu\nu,\alpha\beta}^1(\omega) + i\chi_{\mu\nu,\alpha\beta}^2(\omega)$, then using the Sokhotski-Plemelj theorem

$$\frac{1}{x - x_0 + i0^+} = \text{p.v.} \left(\frac{1}{x - x_0} \right) - i\pi\delta(x - x_0) \quad (30)$$

¹The actual conductivity is the sum of a pole at $\omega = 0$ and a regular part. see e.g. [6] and references therein. Usually we ignore the pole because its weight goes to zero in the thermodynamic limit, unless the system is a perfect conductor or is a superconductor.

we can break up Eq. (28) into

$$\chi_{\mu\nu,\alpha\beta}^1(\omega) = \frac{1}{ZV} \sum_{nm} \langle n|J_{\mu,\alpha}|m\rangle \langle m|J_{\nu,\beta}|n\rangle (e^{-\beta E_n} - e^{-\beta E_m}) \text{p.v.} \left(\frac{1}{\omega + E_n - E_m} \right), \quad (31)$$

$$\chi_{\mu\nu,\alpha\beta}^2(\omega) = \frac{-\pi}{ZV} \sum_{nm} \langle n|J_{\mu,\alpha}|m\rangle \langle m|J_{\nu,\beta}|n\rangle (e^{-\beta E_n} - e^{-\beta E_m}) \delta(\omega\hbar + E_n - E_m). \quad (32)$$

DQMC measures unequal imaginary time (heat) current - (heat) current correlators

$$\chi_{\mu\nu,\alpha\beta}(\tau) = +\frac{1}{V} \langle J_{\mu,\alpha}(\tau) J_{\nu,\beta}(0) \rangle = \frac{+1}{ZV} \sum_{mn} e^{-\beta E_n} e^{\tau(E_n - E_m)} \langle n|J_{\mu,\alpha}|m\rangle \langle m|J_{\nu,\beta}|n\rangle. \quad (33)$$

Comparing Eq. (32) with Eq. (33), we find

$$\chi_{\mu\nu,\alpha\beta}(\tau) = \int_{-\infty}^{\infty} d(\omega\hbar) \frac{e^{-\tau\omega\hbar}}{1 - e^{-\beta\omega\hbar}} \frac{-\chi_{\mu\nu,\alpha\beta}^2(\omega)}{\pi}. \quad (34)$$

Eq. (34) is the key relation that directly relates DQMC measurements in imaginary time to retarded correlators in real frequency.

When $\mu = \nu$ and $\alpha = \beta$, we can show that Eq. (31) and Eq. (32) are purely real, and thus correspond to real and imaginary parts of $\chi_{\mu\mu,\alpha\alpha}^R$, respectively. This means that [c.f. Eq. (25)]

$$\text{Im} [L_{\alpha\alpha}^{(\mu\mu)}(\omega)] = \frac{\chi_{\mu\mu,\alpha\alpha}^1(\omega)}{\omega}, \quad \text{Re} [L_{\alpha\alpha}^{(\mu\mu)}(\omega)] = \frac{-\chi_{\mu\mu,\alpha\alpha}^2(\omega)}{\omega}. \quad (35)$$

so that written out explicitly, we have

$$\chi_{11,xx}(\tau) = \frac{1}{V} \langle J_x(\tau) J_x(0) \rangle = \int_{-\infty}^{\infty} d(\omega\hbar) \frac{\omega e^{-\tau\omega\hbar}}{1 - e^{-\beta\omega\hbar}} \frac{-\chi_{11,xx}^2(\omega)}{\pi\omega} = \int_{-\infty}^{\infty} d(\omega\hbar) \frac{\omega e^{-\tau\omega\hbar}}{1 - e^{-\beta\omega\hbar}} \frac{\text{Re} [L_{xx}^{(11)}(\omega)]}{\pi} \quad (36)$$

and

$$\chi_{22,xx}(\tau) = \frac{1}{V} \langle J_{Q,x}(\tau) J_{Q,x}(0) \rangle = \int_{-\infty}^{\infty} d(\omega\hbar) \frac{\omega e^{-\tau\omega\hbar}}{1 - e^{-\beta\omega\hbar}} \frac{-\chi_{22,xx}^2(\omega)}{\pi\omega} = \int_{-\infty}^{\infty} d(\omega\hbar) \frac{\omega e^{-\tau\omega\hbar}}{1 - e^{-\beta\omega\hbar}} \frac{\text{Re} [L_{xx}^{(22)}(\omega)]}{\pi}. \quad (37)$$

We apply MaxEnt [7] analytic continuation to invert Eqs. (36) and (37), and find the diagonal conductivities $\text{Re} [L_{xx}^{(11)}(\omega)]$ and $\text{Re} [L_{xx}^{(22)}(\omega)]$.

Experimentally, electric conductivity is typically measured under the condition $\nabla T = 0$, so $\sigma = L^{(11)}$, $\text{Re} [\sigma_{xx}(\omega)] = \text{Re} [L_{xx}^{(11)}(\omega)]$, and we obtain the DC value reported in main text by taking $\sigma_{xx}^{\text{DC}} \equiv \text{Re} [\sigma_{xx}(\omega \rightarrow 0)]$.

Thermal conductivity is typically measured under the zero electrical current condition $\mathbf{j} = 0$, so

$$\kappa \equiv \kappa_{zc} = \frac{1}{T} \left(L^{(22)} - L^{(21)} \left(L^{(11)} \right)^{-1} L^{(12)} \right), \quad (38)$$

where the first term may be called the nominal thermal conductivity corresponding to measurements under the condition $\mathbf{E} = 0$,

$$\kappa^0 = \frac{L^{(22)}}{T}. \quad (39)$$

So $\text{Re} [\kappa_{xx}^0(\omega)] = \text{Re} [L_{xx}^{(22)}(\omega)]/T$, and we obtain the DC value reported in main text by taking $\kappa_{xx}^{0,\text{DC}} \equiv \text{Re} [\kappa_{xx}^0(\omega \rightarrow 0)]$. We do this to avoid inverting L matrices with small elements, which will exacerbate statistical noise. The effect of the correction term in Eq. (38) is small [8].

On the other hand, when $J_{\mu,\alpha} \neq J_{\nu,\beta}$, Eq. (31) and Eq. (32) are not necessarily purely real, so do not necessarily correspond to real and imaginary parts of $\chi_{\mu\mu,\alpha\alpha}^R$. In the case of $\alpha = x$, $\beta = y$, and $\mu = \nu$, we can show that $\chi_{\mu\mu,xy}(\tau)$, $\chi_{\mu\mu,xy}^1(\omega)$, and $\chi_{\mu\mu,xy}^2(\omega)$ are all purely imaginary. Using $\chi_{\mu\mu,xy}(\tau)$ as an explicit example, we have

$$\langle J_{\mu,x}(\tau) J_{\mu,y}(0) \rangle = \frac{1}{Z} \sum_{mn} e^{-\beta E_n} e^{\tau(E_n - E_m)} \langle n|J_{\mu,x}|m\rangle \langle m|J_{\mu,y}|n\rangle \quad (40)$$

$$= \frac{1}{Z} \sum_{mn} e^{-\beta E_n} e^{\tau(E_n - E_m)} \overline{\langle n|J_{\mu,y}|m\rangle} \overline{\langle m|J_{\mu,x}|n\rangle} = \overline{\langle J_{\mu,y}(\tau) J_{\mu,x}(0) \rangle} = -\langle J_{\mu,y}(\tau) J_{\mu,x}(0) \rangle, \quad (41)$$

where the last equality used the C_4 symmetry of the square lattice. This means that [c.f. Eq. (25)]

$$\text{Re} \left[L_{xy}^{(\mu\mu)}(\omega) \right] = \frac{i\chi_{\mu\mu,xy}^1(\omega)}{\omega}, \quad \text{Im} \left[L_{xy}^{(\mu\mu)}(\omega) \right] = \frac{i\chi_{\mu\mu,xy}^2(\omega)}{\omega}, \quad (42)$$

so that written out explicitly, we have

$$-i\chi_{22,xy}(\tau) = \frac{-i}{V} \langle J_{Q,x}(\tau) J_{Q,y}(0) \rangle = \int_{-\infty}^{\infty} d(\omega\hbar) \frac{\omega e^{-\tau\omega\hbar}}{1 - e^{-\beta\omega\hbar}} \frac{i\chi_{22,xy}^2(\omega)}{\pi\omega} = \int_{-\infty}^{\infty} d(\omega\hbar) \frac{\omega e^{-\tau\omega\hbar}}{1 - e^{-\beta\omega\hbar}} \frac{\text{Im} \left[L_{xy}^{(22)}(\omega) \right]}{\pi}. \quad (43)$$

As a useful reference, Table 1 summarizes the properties of components of $\chi_{\mu\mu,\alpha\beta}^R(\omega) = \chi_{\mu\mu,\alpha\beta}^1(\omega) + i\chi_{\mu\mu,\alpha\beta}^2(\omega)$

Table 1: Properties of components of $\chi_{\mu\mu,\alpha\beta}$

component	real/imaginary?	symmetry
$\chi_{xx}^1(\omega)$	real	even
$\chi_{xx}^2(\omega)$	real	odd
$\chi_{xy}^1(\omega)$	imaginary	odd
$\chi_{xy}^2(\omega)$	imaginary	even

The off-diagonal spectral weight $\chi_{\mu\mu,xy}^2(\omega)/\omega$ need not be positive over all frequencies, which precludes us from directly applying the standard MaxEnt algorithm to invert Eq. (43). This is a known issue for off-diagonal spectral functions, and in this work, we use two strategies to tackle this, which we call the subtraction method (Section S4.1) and the proxy method (Section S4.2), respectively.

S4.1 Subtraction method

The subtraction method adopts the strategies of [9, 10]. Namely, we perform analytic continuation on the composite object $\chi_{\mu\mu,xx}(\tau) - i\chi_{\mu\mu,xy}(\tau)$, subtract out the longitudinal response $\chi_{\mu\mu,xx}^2(\omega)$ to obtain the transverse response $\chi_{\mu\mu,xy}^2(\omega)$, using the relation

$$\begin{aligned} \chi_{\mu\mu,xx}(\tau) - i\chi_{\mu\mu,xy}(\tau) &= \frac{1}{V} \langle J_{\mu,x}(\tau) J_{\mu,x}(0) \rangle + \frac{-i}{V} \langle J_{\mu,x}(\tau) J_{\mu,y}(0) \rangle \\ &= \int_{-\infty}^{\infty} d(\omega\hbar) \frac{\omega e^{-\tau\omega\hbar}}{1 - e^{-\beta\omega\hbar}} \left[\frac{-\chi_{\mu\mu,xx}^2(\omega)}{\pi\omega} + \frac{i\chi_{\mu\mu,xy}^2(\omega)}{\pi\omega} \right] \end{aligned} \quad (44)$$

$$= \int_{-\infty}^{\infty} d(\omega\hbar) \frac{\omega e^{-\tau\omega\hbar}}{1 - e^{-\beta\omega\hbar}} \left[\frac{\text{Re} \left[L_{xx}^{(\mu\mu)}(\omega) \right]}{\pi} + \frac{\text{Im} \left[L_{xy}^{(\mu\mu)}(\omega) \right]}{\pi} \right]. \quad (45)$$

As long as the off-diagonal spectral weight is small, this procedure allows it to “piggyback” on a large positive diagonal spectral weight and allow MaxEnt to proceed as usual. This entails performing two MaxEnt fits, and subtracting them to obtain our desired result.

Because the analytic continuation relation Eq. (34) only allows us to obtain $\chi_{\mu\mu,xy}^2(\omega)$ or $\text{Im} \left[L_{xy}^{(\mu\mu)}(\omega) \right]$, we also need to perform a Kramers-Kronig transform after the subtraction of two MaxEnt spectra to obtain

$$\text{Re} \left[L_{xy}^{(\mu\mu)}(\omega) \right] = \frac{i\chi_{\mu\mu,xy}^1(\omega)}{\omega} = \frac{1}{\omega} \text{p.v.} \int_{-\infty}^{\infty} \frac{i\chi_{\mu\mu,xy}^2(\omega')}{\omega' - \omega} \frac{d\omega'}{\pi} = \frac{1}{\omega} \text{p.v.} \int_{-\infty}^{\infty} \frac{\omega \text{Im} \left[L_{xy}^{(\mu\mu)}(\omega') \right]}{\omega' - \omega} \frac{d\omega'}{\pi}. \quad (46)$$

More specifically, we are interested in the DC value, obtained by

$$\lim_{\omega \rightarrow 0} \text{Re} \left[L_{xy}^{(\mu\mu)}(\omega) \right] = i \text{p.v.} \int \frac{d\omega'}{\pi} \frac{d}{d\omega} \frac{\chi_{\mu\mu,xy}^2(\omega')}{\omega' - \omega} \Big|_{\omega=0} = i \int \frac{d\omega'}{\pi} \frac{\chi_{\mu\mu,xy}^2(\omega')}{\omega'^2}. \quad (47)$$

Some typical spectra and corresponding DC result obtained via this subtraction procedure are shown in Fig. S2.

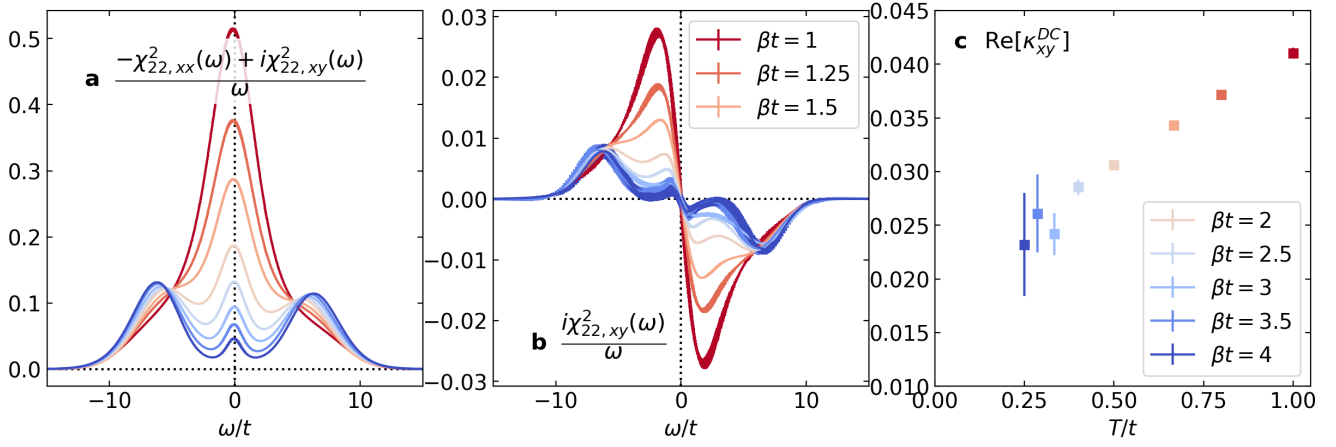


Figure S2: Examples of MaxEnt subtraction method for obtaining the thermal Hall conductivity. **a** The result of analytically continuing the composite object, Eq. (44), **b** The off-diagonal spectra, **c** the result after Kramers-Kronig transform, Eq. (47). Next nearest neighbor hopping $t'/t = -0.1$, Hubbard $U/t = 6$, magnetic field strength $\Phi/\Phi_0 = 4/64$. Error bars denote one standard deviation of the mean, obtained via bootstrap resampling.

Once we have obtained $\kappa_{xy}^{\text{DC}} = \lim_{\omega \rightarrow 0} \text{Re} [L_{xy}^{(22)}(\omega)]/T$ as outlined above, and κ_{xx}^{DC} via standard MaxEnt Eq. (37), we can in turn calculate the thermal Hall angle $\theta_{\text{th,H}}$, defined as

$$\tan \theta_{\text{th,H}} = \frac{\kappa_{xy}^{\text{DC}}}{\kappa_{xx}^{\text{DC}}}, \quad (48)$$

and the Hall coefficient, $R_{\text{th,H}} = \frac{\nabla T_y}{j_{q,x} B}$, defined as

$$R_{\text{th,H}} = \frac{1}{B} \frac{\kappa_{xy}^{\text{DC}}}{(\kappa_{xx}^{\text{DC}})^2 + (\kappa_{xy}^{\text{DC}})^2}. \quad (49)$$

S4.2 Proxy method

We have argued in an earlier work [11] about the properties of $\chi_{11,xy}(\tau)$; the situation is entirely analogous for thermal conductivity. $\chi_{22,xy}(\tau)$ is purely imaginary, and antisymmetric about $\tau = \beta/2$. By considering the Fourier transformed imaginary frequency correlator

$$\chi_{\mu\mu,\alpha\beta}(i\omega_n) = \int_0^\beta d\tau \chi_{\mu\mu,\alpha\beta}(\tau) e^{i\omega_n \tau} = \frac{1}{ZV} \sum_{mn} \frac{e^{-\beta E_n} - e^{-\beta E_m}}{i\omega_n + E_n - E_m} \langle n | J_{\mu,\alpha} | m \rangle \langle m | J_{\nu,\beta} | n \rangle \quad (50)$$

we define [11, 12]

$$L_{xx}^{(\mu\mu)}(i\omega_n) = \frac{\chi_{\mu\mu,xx}(i\omega_n) - \chi_{\mu\mu,xx}(i\omega_n = 0)}{\omega_n}, \quad (51)$$

$$L_{xy}^{(\mu\mu)}(i\omega_n) = \frac{\chi_{\mu\mu,xy}(i\omega_n)}{\omega_n}, \quad (52)$$

so that we obtain the finite-field version of Eq. (12) in [11] for the thermal Hall coefficient:

$$R_{\text{th,H}}^{\text{M1}}(i\omega_n) = \frac{1}{B} \frac{\chi_{22,xy}(i\omega_n) \omega_n T}{(\chi_{22,xx}(i\omega_n) - \chi_{22,xx}(0))^2 + \chi_{22,xy}(i\omega_n)^2}. \quad (53)$$

This formula Eq. (53) is exact for the DC thermal Hall coefficient at zero temperature,

$$\lim_{i\omega_n \rightarrow 0} R_{\text{th,H}}^{\text{M1}}(i\omega_n) = \lim_{\omega \rightarrow 0} R_{\text{th,H}}(\omega) = R_{\text{th,H}}^{\text{DC}}. \quad (54)$$

At finite temperatures, we are only able to calculate Eq. (53) for nonzero Matsubara frequencies, so we take the value of $R_{\text{th,H}}^{\text{M1}}(i\omega_n)$ at the lowest nonzero Matsubara frequency $\omega_1 = 2\pi/\beta$ as a proxy for $R_{\text{th,H}}^{\text{DC}}$. As long as $R_{\text{th,H}}^{\text{M1}}(i\omega_n)$ is well-behaved as a function of imaginary frequency, we have some confidence that its value at $\omega_0 = 0$ and $\omega_1 = 2\pi/\beta$ do not differ significantly.

Some typical examples of χ_{22} and $R_{\text{th,H}}$ results obtained via this proxy procedure are shown in Fig. S3.

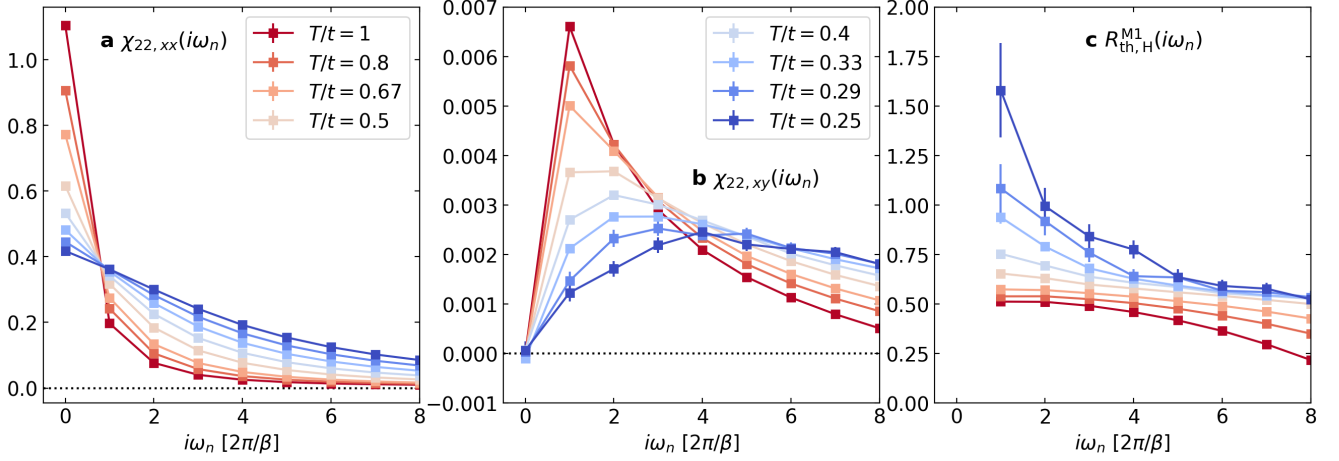


Figure S3: Examples of proxy method for obtaining the thermal Hall conductivity. Next nearest neighbor hopping $t'/t = -0.1$, Hubbard $U/t = 6$, magnetic field strength $\Phi/\Phi_0 = 1/64$. Error bars denote one standard deviation of the mean, obtained via jackknife resampling.

Once we have obtained $R_{\text{th,H}}$ as outlined above, and κ_{xx}^{DC} via standard MaxEnt Eq. (37), we can use Eqs. (48) and (49) to solve for $\tan(\theta_{\text{th,H}})$

$$\frac{\tan(\theta_{\text{th,H}})}{1 + \tan^2(\theta_{\text{th,H}})} = \kappa_{xx}^{\text{DC}} \cdot B \cdot R_{\text{th,H}} \quad (55)$$

and derive

$$\kappa_{xy}^{\text{DC}} = \kappa_{xx}^{\text{DC}} \tan(\theta_{\text{th,H}}) \quad (56)$$

S5 Energy magnetization term

By introducing the pseudogravitational potential in (22), there is an additional contribution to the heat current density $\mathbf{j}_q(\mathbf{r})$ stemming from the fact that ψ couples to the energy density h_i itself [13, 14]. In the DC limit, this extra contribution modifies the thermal conductivity by $\kappa_{xy} = \kappa_{xy,\text{Kubo}} + \kappa_{xy,\text{EM}}$, where $\kappa_{xy,\text{Kubo}}$ is the usual Kubo term discussed in Section S4, and $\kappa_{xy,\text{EM}}$ is the energy magnetization correction, given by

$$\kappa_{xy,\text{EM}} = \frac{2}{TV} \int d\mathbf{r} \langle r_y j_{Q,x}(\mathbf{r}) \rangle_0 = \frac{2}{T} \frac{1}{i} \left\langle \left[\frac{\partial j_{Q,x}(\mathbf{q})}{\partial q_y} \right]_{\mathbf{q}=0} \right\rangle_0. \quad (57)$$

Since we consider periodic boundary conditions, position \mathbf{r} is not well-defined. In other words, the value of $\kappa_{xy,\text{EM}}$ in general depends on the choice in origin. Nonetheless, we see in Fig. S4 that the overall magnitude of $\kappa_{xy,\text{EM}}/T$ systematically decreases as a function of system size regardless of choice in origin. In contrast, the proxy used to compute $\kappa_{xy,\text{Kubo}}/T$ does not drastically change as a function of system size, as shown in Fig. S5. Moreover, on a 8×8 cluster, the maximum value for the energy magnetization correction is negligible compared to $\kappa_{xy,\text{Kubo}}/T$ at all temperatures. Thus, for the results in the main text, we only consider the Kubo contribution.

S6 Proof of zero transverse responses when $t' = 0$

Consider the Hubbard-Hofstadter Hamiltonian on a bipartite lattice at half filling, and define the charge conjugation transform as:

$$c_{i\sigma} \rightarrow (-1)^i c_{i\sigma}^\dagger, \quad c_{i\sigma}^\dagger \rightarrow (-1)^i c_{i\sigma}, \quad (58)$$

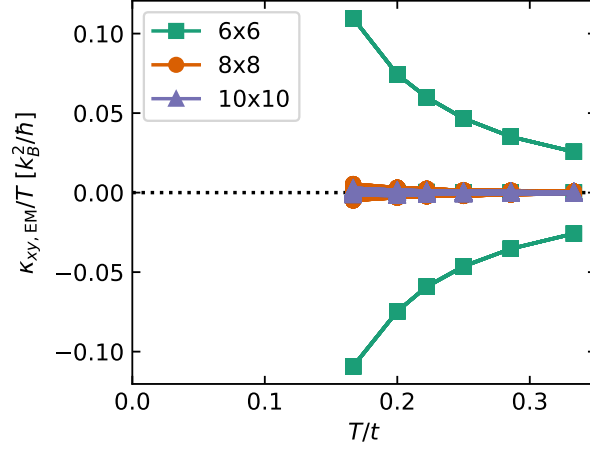


Figure S4: Finite size dependence of the energy magnetization correction $\kappa_{xy,\text{EM}}/T$, Eq. (57), calculated under periodic boundary conditions for $U/t = 6$, $t'/t = -0.1$. The magnetic field strengths are $\Phi/\Phi_0 = 1/36$, $\Phi/\Phi_0 = 1/64$, and $\Phi/\Phi_0 = 1/100$ for 6×6 , 8×8 , and 10×10 respectively. For each system size, $\kappa_{xy,\text{EM}}/T$ computed for all possible choices in origin are shown.

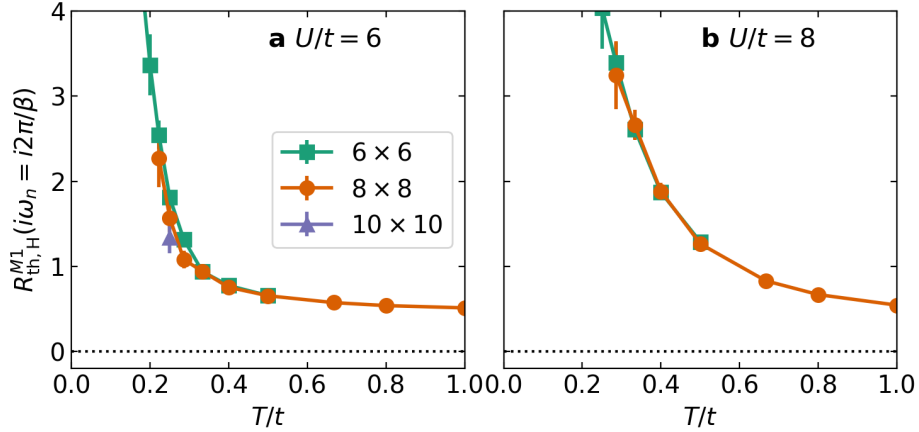


Figure S5: Finite size dependence of $R_{\text{th,H}}^{\text{M1}}$ proxy for Hubbard interaction **a** $U/t = 6$ and **b** $U/t = 8$, both with $t'/t = -0.1$ at half filling $\langle n \rangle = 1$. The magnetic field strength is $\Phi/\Phi_0 = 1/36$ on a 6×6 cluster, $\Phi/\Phi_0 = 3/64$ on a 8×8 cluster, and $\Phi/\Phi_0 = 2/100$ on a 10×10 cluster.

. Both panels share the same legend.

where sign of prefactor $(-1)^i$ depending on sublattice. This is a unitary transformation. Without an applied magnetic field, the Hamiltonian is symmetric under charge conjugation: $H = CHC^{-1}$. In the presence of a magnetic field, the Hamiltonian is not invariant under charge conjugation, but instead transforms under charge conjugation as

$$H(\mathbf{A}) \rightarrow CH(\mathbf{A})C^{-1} = H(-\mathbf{A}). \quad (59)$$

The electrical current operator Eq. (1) and heat current operator Eq. (19) (with $\mu = 0$ at half filling) transforms under charge conjugation as²:

$$\mathbf{J}(\mathbf{A}) \rightarrow C\mathbf{J}(\mathbf{A})C^{-1} = -\mathbf{J}(-\mathbf{A}) \quad (60)$$

$$\mathbf{J}_Q(\mathbf{A}) \rightarrow C\mathbf{J}_Q(\mathbf{A})C^{-1} = \mathbf{J}_Q(-\mathbf{A}). \quad (61)$$

This means the transverse current-current correlator in imaginary time satisfies:

$$\begin{aligned} \chi_{11,xy}(\mathbf{A}) &= \langle J_x(\mathbf{A}, \tau) J_y(\mathbf{A}) \rangle = \text{Tr} \left[e^{-\beta H(\mathbf{A})} e^{\tau H(\mathbf{A})} J_x(\mathbf{A}) e^{-\tau H(\mathbf{A})} J_y(\mathbf{A}) \right] / \text{Tr} \left[e^{-\beta H(\mathbf{A})} \right] \\ &= \text{Tr} \left[C e^{-\beta H(\mathbf{A})} e^{\tau H(\mathbf{A})} C^{-1} C J_x(\mathbf{A}) C^{-1} C e^{-\tau H(\mathbf{A})} C^{-1} C J_y(\mathbf{A}) C^{-1} \right] / \text{Tr} \left[C e^{-\beta H(\mathbf{A})} C^{-1} \right] \\ &= \text{Tr} \left[e^{-\beta H(-\mathbf{A})} e^{\tau H(-\mathbf{A})} J_x(-\mathbf{A}) e^{-\tau H(-\mathbf{A})} J_y(-\mathbf{A}) \right] / \text{Tr} \left[e^{-\beta H(-\mathbf{A})} \right] \\ &= \chi_{11,xy}(-\mathbf{A}). \end{aligned} \quad (62)$$

Analogously, the transverse heat current-heat current correlator in imaginary time obeys

$$\chi_{22,xy}(\mathbf{A}) = \chi_{22,xy}(-\mathbf{A}). \quad (63)$$

For the sake of completeness, the charge current-heat current correlator in imaginary time obeys

$$\begin{aligned} \chi_{12,xx}(\mathbf{A}) &= \langle J_x(\mathbf{A}, \tau) J_{Q,x}(\mathbf{A}) \rangle = \text{Tr} \left[e^{-\beta H(\mathbf{A})} e^{\tau H(\mathbf{A})} J_x(\mathbf{A}) e^{-\tau H(\mathbf{A})} J_{Q,x}(\mathbf{A}) \right] / \text{Tr} \left[e^{-\beta H(\mathbf{A})} \right] \\ &= \text{Tr} \left[C e^{-\beta H(\mathbf{A})} e^{\tau H(\mathbf{A})} C^{-1} C J_x(\mathbf{A}) C^{-1} C e^{-\tau H(\mathbf{A})} C^{-1} C J_{Q,x}(\mathbf{A}) C^{-1} \right] / \text{Tr} \left[C e^{-\beta H(\mathbf{A})} C^{-1} \right] \\ &= -\text{Tr} \left[e^{-\beta H(-\mathbf{A})} e^{\tau H(-\mathbf{A})} J_x(-\mathbf{A}) e^{-\tau H(-\mathbf{A})} J_{Q,x}(-\mathbf{A}) \right] / \text{Tr} \left[e^{-\beta H(-\mathbf{A})} \right] \\ &= -\chi_{12,xx}(-\mathbf{A}). \end{aligned} \quad (64)$$

In the presence of external magnetic field, The thermoelectric response coefficients obey the Onsager relations [15]

$$L_{\alpha\beta}^{(\mu\nu)}(B) = L_{\beta\alpha}^{(\nu\mu)}(-B). \quad (65)$$

Combining Eq. (65) with Eqs. (62) to (64) and Kubo formulas, we find that at half-filling, with $t' \neq 0$, the Hubbard-Hofstadter Hamiltonian satisfies

$$\alpha_{xx}(B) = \sigma_{xy}(B) = \kappa_{xy}(B) = 0. \quad (66)$$

S7 Magnon-magnon scattering

S7.1 Holstein-Primakoff expansion

To study the effects of magnon-magnon interactions, we consider the low-energy effective spin model

$$H_{\text{eff}} = J_1 \sum_{\langle ij \rangle} \mathbf{S}_i \cdot \mathbf{S}_j + J_2 \sum_{\langle\langle ij \rangle\rangle} \mathbf{S}_i \cdot \mathbf{S}_j + J_\chi \sum_{\Delta_{ijk}} \mathbf{S}_i \cdot (\mathbf{S}_j \times \mathbf{S}_k), \quad (67)$$

and perform a large S expansion around a Neel state. We want to study perturbations of the spins away from the local z axes, so we must first perform local rotations to each site. Taking $\mathbf{S}_i = R_i \tilde{\mathbf{S}}_i$ where $R \in \text{SO}(3)$, we can write the Hamiltonian in the rotated basis

$$H = \sum_{i,j \in i} \tilde{\mathbf{S}}_i^T \tilde{H}_{ij}^{(2)} \tilde{\mathbf{S}}_j + \sum_{\Delta_{ijk}} \epsilon_{\alpha\beta\gamma} \tilde{S}_i^\alpha \tilde{S}_j^\beta \tilde{S}_k^\gamma \tilde{H}_{ijk}^{(3),\alpha\beta\gamma}, \quad \text{where } \tilde{H}_{ijk}^{(3),\alpha\beta\gamma} = R_i^\alpha R_j^\beta R_k^\gamma H_{ijk}^{(3),\alpha\beta\gamma}, \quad (68)$$

²We noticed an error in the supplementary material of Ref. [8], where after the particle-hole transformation, the current operators should change as $J_K \rightarrow J_{\bar{K}}$, $J_P \rightarrow J_{\bar{P}}$, and $J \rightarrow -J$.

and $H_{ij}^{(2)}$ and $H_{ij}^{(3)}$ are tensors encoding the quadratic and cubic spin interactions. In this basis, we can perform local Holstein-Primakoff (HP) transformations

$$\tilde{S}_i^z = S - a_i^\dagger a_i = S - n_i \quad (69)$$

$$\tilde{S}_i^x = \frac{\sqrt{2S - n_i} a_i + a_i^\dagger \sqrt{2S - n_i}}{2} \approx \sqrt{\frac{S}{2}} (a_i + a_i^\dagger) \quad (70)$$

$$\tilde{S}_i^y = \frac{\sqrt{2S - n_i} a_i - a_i^\dagger \sqrt{2S - n_i}}{2i} \approx -i\sqrt{\frac{S}{2}} (a_i - a_i^\dagger). \quad (71)$$

After performing the substitutions, the quadratic Hamiltonian is given by

$$H^{(2)} = \sum_{\mathbf{k}} \varepsilon_{\mathbf{k}} \left(\alpha_{\mathbf{k}}^\dagger \alpha_{\mathbf{k}} + \beta_{\mathbf{k}}^\dagger \beta_{\mathbf{k}} \right), \quad (72)$$

where $\alpha_{\mathbf{k}}$ and $\beta_{\mathbf{k}}$ are operators for the Bogoliubov quasiparticles, related to the magnon quasiparticles by

$$a_{A,\mathbf{k}} = u_{\mathbf{k}} \alpha_{\mathbf{k}} + v_{\mathbf{k}} \beta_{-\mathbf{k}}^\dagger \quad (73)$$

$$a_{B,\mathbf{k}} = u_{\mathbf{k}} \beta_{\mathbf{k}} + v_{\mathbf{k}} \alpha_{-\mathbf{k}}^\dagger \quad (74)$$

$$a_{A,\mathbf{k}}^\dagger = u_{\mathbf{k}} \alpha_{\mathbf{k}}^\dagger + v_{\mathbf{k}} \beta_{-\mathbf{k}} \quad (75)$$

$$a_{B,\mathbf{k}}^\dagger = u_{\mathbf{k}} \beta_{\mathbf{k}}^\dagger + v_{\mathbf{k}} \alpha_{-\mathbf{k}}, \quad (76)$$

where $u_{\mathbf{k}} = \cosh \theta_{\mathbf{k}}$, $v_{\mathbf{k}} = \sinh \theta_{\mathbf{k}}$, $\tanh 2\theta_{\mathbf{k}} = -\gamma_{\mathbf{k}}$, and $\gamma_{\mathbf{k}} = \frac{1}{2} (\cos(k_x) + \cos(k_y))$. The (degenerate) energies are given by

$$\varepsilon_{\mathbf{k}} = 4J_1 S \phi_{\mathbf{k}} \sqrt{1 - \left(\frac{\gamma_{\mathbf{k}}}{\phi_{\mathbf{k}}} \right)^2}, \quad (77)$$

where

$$\phi_{\mathbf{k}} = 1 + \frac{J_2}{J_1} \left[\frac{1}{2} (\cos(k_x + k_y) + \cos(k_x - k_y)) - 1 \right]. \quad (78)$$

Note that J_χ does not contribute to the quadratic Hamiltonian; rather, it contributes quartic terms (to order S) to the Hamiltonian in the form of

$$H^{(4)} = \sum_{\mathbf{k}, \mathbf{k}_1, \mathbf{k}_2, \mathbf{k}_3} \delta_{\mathbf{k}+\mathbf{k}_1+\mathbf{k}_2+\mathbf{k}_3} W_{\mathbf{k}, \mathbf{k}_1, \mathbf{k}_2, \mathbf{k}_3}^{\alpha\beta\gamma\delta} \psi_{\mathbf{k}}^\alpha \psi_{\mathbf{k}_1}^\beta \psi_{\mathbf{k}_2}^\gamma \psi_{\mathbf{k}_3}^\delta, \quad (79)$$

where $\psi_{\mathbf{k}} = (\alpha_{\mathbf{k}}, \beta_{\mathbf{k}}, \alpha_{-\mathbf{k}}^\dagger, \beta_{-\mathbf{k}}^\dagger)$. The interaction vertices $W_{\mathbf{k}, \mathbf{k}_1, \mathbf{k}_2, \mathbf{k}_3}^{\alpha\beta\gamma\delta}$ are terms of the form

$$\frac{iSJ_\chi}{N} \eta_{\mathbf{k}} \sum_{\{\delta_j, \delta_k\} \in \Delta} [\cos(\mathbf{q}_1 \cdot \delta_j + \mathbf{q}_2 \cdot \delta_k) \pm \cos(\mathbf{q}_3 \cdot \delta_j + \mathbf{q}_4 \cdot \delta_k)], \quad (80)$$

where \mathbf{q}_n are linear combinations of $\mathbf{k}, \mathbf{k}_1, \mathbf{k}_2, \mathbf{k}_3$, δ_j and δ_k are displacement vectors to the j and k sites within a triangular plaquette, and $\eta_{\mathbf{k}}$ are various combinations of four $u_{\mathbf{k}}$ and $v_{\mathbf{k}}$. Since $u_{\mathbf{k}}$ and $v_{\mathbf{k}}$ are real, the vertices $W_{\mathbf{k}, \mathbf{k}_1, \mathbf{k}_2, \mathbf{k}_3}^{\alpha\beta\gamma\delta}$ are purely imaginary. We may also consider quartic interactions at order $1/S$ coming from the J_1 and J_2 interactions of similar form, which are purely real. Many of these processes will contribute to longitudinal transport, but only some will contribute to the Hall transport.

S7.2 Mean-field theory analysis

First, we explore if spin interactions incorporated at the mean-field level to the magnon Hamiltonian is sufficient for “escaping” the no-go theorem and observing a finite thermal Hall signal.

We start with spin-wave theory on top of Neel order. The cubic spin interaction, which breaks TRS at the

Hamiltonian level, is given as

$$H_\chi = \frac{1}{2iS^3} \sum_{\triangle_{ijk}} S_i^z (S_j^- S_k^+ - S_j^+ S_k^-) + S_j^z (S_k^- S_i^+ - S_k^+ S_i^-) + S_k^z (S_i^- S_j^+ - S_j^- S_i^+) \quad (81)$$

$$= \frac{1}{iS^2} \sum_{j \in A} \sum_{\sigma, \sigma' \in \{\pm\}} \sigma \sigma' \left(\left[a_{B,j-\sigma\hat{x}}^\dagger a_{B,j-\sigma\hat{x}} a_{A,j}^\dagger a_{B,j-\sigma'\hat{y}}^\dagger - H.c. \right] - (\hat{x} \leftrightarrow \hat{y}) \right) - \left(a_{A,j}^\dagger a_{A,j} a_{B,j-\sigma\hat{y}}^\dagger a_{B,j-\sigma'\hat{x}}^\dagger - H.c. \right) \quad (82)$$

$$+ \frac{1}{iS^2} \sum_{j \in B} (A \leftrightarrow B), \quad (83)$$

where we sum over all triangles with i, j , and k labeling the vertices in a clockwise order. In the second line we have performed the HP transformation and dropped terms with more than four magnons, and A and B denote the A and B sublattice. There is no quadratic contribution from this term to the SWT Hamiltonian, as stated by the no-go theorem [16].

We now see if the term contributes at the mean-field level. We perform the mean-field decoupling allowing as much freedom as possible. However, because the DQMC results see the thermal Hall effect even for extremely small t' , we assume that any signal is a feature of the Neel-ordered phase and therefore we should not break any symmetry present in the phase that is not explicitly broken by the perturbation.

We define the mean-fields

$$\Theta_{r'-r}^{X^\pm Y^\pm} = \langle a_{A,r}^\pm a_{B,r'}^\pm \rangle \quad (84)$$

e.g. $\Theta_x^{A+B-} = \langle a_{A,j}^\dagger a_{B,j+x} \rangle$. Due to not wanting to break additional symmetry, we only allow for magnetization conserving terms: $a_{A,i}^\dagger a_{A,j}$, $a_{B,i}^\dagger a_{B,j}$, $a_{A,i} a_{B,j}$, and $a_{A,i}^\dagger a_{B,j}^\dagger$. With this restriction, the only mean-fields that appear are

$$\begin{aligned} \Theta_{nn}^{A+,B+} &= \Theta_{-\hat{x}}^{A+B+} = \Theta_{\hat{y}}^{A+B+} = \Theta_{-\hat{y}}^{A+B+}; \\ \Theta_{nnn}^{B-,B+} &= \Theta_{\hat{y}+\hat{x}}^{B-B+} = \Theta_{\hat{y}-\hat{x}}^{B-B+}; \quad \Theta_{nnn}^{A-,A+} = \Theta_{\hat{y}+\hat{x}}^{A-A+} = \Theta_{\hat{y}-\hat{x}}^{A-A+}; \quad \Delta S = \Theta_0^{A+A-}, \Theta_0^{B+B-}; \end{aligned} \quad (85)$$

where we made use of C_4 symmetry to group terms that all should take the same value. Note that $(\Theta_{nnn}^{X-X+})^* = (\Theta_{\hat{y}+\hat{x}}^{B-B+})^* = \Theta_{-\hat{y}-\hat{x}}^{B-B+} = \Theta_{\hat{y}+\hat{x}}^{B-B+}$ using C_4 symmetry.

After mean-field decoupling the Hamiltonian and performing a Fourier transform, we arrive at

$$\begin{aligned} iS^2 H_\chi &= C_\chi + \sum_{\mathbf{k}} Q_{AA}(\mathbf{k}) a_{A,\mathbf{k}}^\dagger a_{A,\mathbf{k}} + Q_{BB}(\mathbf{k}) a_{B,\mathbf{k}}^\dagger a_{B,\mathbf{k}} + Q_{AB}(\mathbf{k}) a_{A,-\mathbf{k}} a_{B,\mathbf{k}} + Q_{AB}(\mathbf{k})^* a_{A,-\mathbf{k}}^\dagger a_{B,\mathbf{k}}^\dagger \\ Q_{AA}(\mathbf{k}) &= \sum_{\sigma\sigma'} \sigma\sigma' \left[\Theta_{-\sigma\hat{x}}^{A-B-} e^{i\mathbf{k}\cdot(\sigma'\hat{y}-\sigma\hat{x})} - \Theta_{-\sigma\hat{x}}^{A+B+} e^{i\mathbf{k}\cdot(\sigma\hat{x}-\sigma'\hat{y})} + \Theta_{-\sigma'\hat{y}}^{A+B+} e^{i\mathbf{k}\cdot(\sigma'\hat{y}-\sigma\hat{x})} - \Theta_{-\sigma'\hat{y}}^{A-B-} e^{i\mathbf{k}\cdot(\sigma\hat{x}-\sigma'y)} \right] = 0 \\ Q_{BB}(\mathbf{k}) &= \sum_{\sigma\sigma'} \sigma\sigma' \left[\Theta_{-\sigma\hat{x}}^{B-A-} e^{i\mathbf{k}\cdot(\sigma'\hat{y}-\sigma\hat{x})} - \Theta_{-\sigma\hat{x}}^{B+A+} e^{i\mathbf{k}\cdot(\sigma\hat{x}-\sigma'\hat{y})} + \Theta_{-\sigma'\hat{y}}^{B+A+} e^{i\mathbf{k}\cdot(\sigma'\hat{y}-\sigma\hat{x})} - \Theta_{-\sigma'\hat{y}}^{B-A-} e^{i\mathbf{k}\cdot(\sigma\hat{x}-\sigma'\hat{y})} \right] = 0 \\ Q_{AB}(\mathbf{k}) &= \sum_{\sigma\sigma'} \sigma\sigma' \left[e^{ik_x\sigma} (\Theta_{\sigma'\hat{y}-\sigma\hat{x}}^{B+B-} - \Theta_{\sigma'\hat{y}}^{A+B+}) + e^{ik_y\sigma'} (\Theta_{\sigma\hat{x}}^{A+B+} - \Theta_{\sigma\hat{x}-\sigma'\hat{y}}^{B+B-}) \right. \\ &\quad \left. + e^{-ik_x\sigma} (\Theta_{\sigma'\hat{y}-\sigma\hat{x}}^{A+A-} - \Theta_{\sigma'\hat{y}}^{B+A+}) + e^{-ik_y\sigma'} (\Theta_{\sigma\hat{x}}^{B+A+} - \Theta_{\sigma\hat{x}-\sigma'\hat{y}}^{A+A-}) \right] \\ &= \sum_{\sigma,\sigma'} \sigma\sigma' \left[e^{ik_x\sigma} (\Theta_{nnn}^{B+B-} - \Theta_{nnn}^{A+A-}) + e^{ik_y\sigma'} (\Theta_{nnn}^{A+A-} - \Theta_{nnn}^{B+B-}) \right] = 0 \end{aligned} \quad (86)$$

where $C_\chi = 0$ through a similar manipulations. We used that $\Theta_{nnn}^{B+B-} = \Theta_{nnn}^{A+A-}$, since, if there were spontaneous sublattice symmetry breaking, it would be detectable in DQMC in long-range correlators, but the numerical results preserve translation symmetry. Therefore there is no contribution to the quadratic magnon Hamiltonian from H_χ at the mean-field level. This derivation excludes an emergent Berry curvature explanation for the observed thermal Hall signal and instead suggests that magnon scattering as the only possible mechanism.

S7.3 Time Reversal Symmetry

Before we proceed with the scattering theory, we first examine the time-reversal symmetry (TRS) of the Bogoliubov Hamiltonian since breaking TRS allows for a finite thermal Hall coefficient. We emphasize here that TRS is defined

with respect to the Bogoliubov operators rather than the usual spin operators. Although a spin Hamiltonian may (may not) be TRS, the corresponding magnon Hamiltonian can break (preserve) TRS. For example, a Zeeman field breaks TRS in the spin language, but is preserved in HP operators. The TR operator \mathcal{T} in the HP language can be defined as

$$\mathcal{T}\alpha_{\mathbf{k}}\mathcal{T}^{-1} = \alpha_{-\mathbf{k}} \quad (87)$$

$$\mathcal{T}\alpha_{\mathbf{k}}^{\dagger}\mathcal{T}^{-1} = \alpha_{-\mathbf{k}}^{\dagger} \quad (88)$$

$$\mathcal{T}\beta_{\mathbf{k}}\mathcal{T}^{-1} = \beta_{-\mathbf{k}} \quad (89)$$

$$\mathcal{T}\beta_{\mathbf{k}}^{\dagger}\mathcal{T}^{-1} = \beta_{-\mathbf{k}}^{\dagger}. \quad (90)$$

Since \mathcal{T} is antiunitary, it also contains complex conjugation $\mathcal{T}c\mathcal{T}^{-1} = c^*$. The Hamiltonian is TR invariant if $H = \mathcal{T}H\mathcal{T}^{-1}$. Thus, the conditions for our Hamiltonian to be TR symmetric are:

$$\begin{aligned} H^{(2)} : \quad & \varepsilon_{\mathbf{k}} = \varepsilon_{-\mathbf{k}} \\ H^{(4)} : \quad & \left(W_{\mathbf{k},\mathbf{k}_1,\mathbf{k}_2,\mathbf{k}_3}^{\alpha\beta\gamma\delta} \right)^* = W_{-\mathbf{k},-\mathbf{k}_1,-\mathbf{k}_2,-\mathbf{k}_3}^{\alpha\beta\gamma\delta}. \end{aligned}$$

In our case, $\left(W_{\mathbf{k},\mathbf{k}_1,\mathbf{k}_2,\mathbf{k}_3}^{\alpha\beta\gamma\delta} \right)^* = -W_{-\mathbf{k},-\mathbf{k}_1,-\mathbf{k}_2,-\mathbf{k}_3}^{\alpha\beta\gamma\delta}$, for the vertices involving the J_{χ} , thus it is possible to generate a finite thermal Hall effect.

S7.4 Semi-Classical Boltzmann Transport

We use semi-classical Boltzmann transport theory to compute the thermal Hall due to magnon-magnon scattering [17]. From Fourier's law (i.e., a restatement of Eq. 24), the thermal conductivity is related to the magnon heat current by

$$j_q^{\mu} = -\kappa^{\mu\nu} \partial_{\nu} T. \quad (91)$$

The magnon heat current density is given by

$$\mathbf{j}_q = \frac{1}{V} \sum_{\mathbf{k}} \varepsilon_{\mathbf{k}} \mathbf{v}_{\mathbf{k}} N_{\mathbf{k}}, \quad (92)$$

where $\varepsilon_{\mathbf{k}}$ is the free magnon dispersion, $\mathbf{v}_{\mathbf{k}} = \partial\varepsilon_{\mathbf{k}}/\partial\mathbf{k}$ is the magnon group velocity, and V is the volume of the system. $N_{\mathbf{k}} = N_{\mathbf{k}}(t, \mathbf{r}(t))$ is the out of equilibrium magnon distribution function and can be computed using the semi-classical Boltzmann equation (BE)

$$\mathbf{v}_{\mathbf{k}} \cdot \nabla T \frac{\partial N_{\mathbf{k}}}{\partial T} = I_{\mathbf{k}}^{\text{coll}}, \quad (93)$$

where $I_{\mathbf{k}}^{\text{coll}}$ is the collision integral. The left hand side represents the diffusion due to the temperature gradient and the right hand side represents the scattering rate between the magnons mediated by magnon-magnon interactions. The collision integral is

$$I_{\mathbf{k}}^{\text{coll}} = \sum_{\mathbf{k}'} \Gamma_{\mathbf{k}}[\{N_{\mathbf{k}'}\}] = \sum_{\mathbf{k}'} \left(\Gamma_{\mathbf{k}}^{\text{in}}[\{N_{\mathbf{k}'}\}] - \Gamma_{\mathbf{k}}^{\text{out}}[\{N_{\mathbf{k}'}\}] \right), \quad (94)$$

where $\Gamma_{\mathbf{k}}[\{N_{\mathbf{k}'}\}]$ are all the scattering processes due to magnons with a momentum \mathbf{k}' . We can compute $\Gamma_{\mathbf{k}}$ using Fermi's golden rule, or

$$\Gamma_{\text{if}}[\{N_{\mathbf{k}'}\}] = \frac{2\pi}{\hbar} |T_{\text{if}}|^2 \delta(E_i - E_f), \quad (95)$$

where the transition matrix T_{if} is given by

$$T_{\text{if}} = \langle f | T | i \rangle, \quad (96)$$

$$T = H_{\text{int}} + H_{\text{int}} \left(\sum_{\nu} \frac{|\nu\rangle\langle\nu|}{E_i - E_{\nu} + i\eta} \right) H_{\text{int}} + \dots, \quad \eta > 0 \quad (97)$$

and ν labels the intermediate states. We make use of the relations

$$\begin{aligned} \alpha_{\mathbf{k}}^{\dagger}(\beta_{\mathbf{k}}^{\dagger})|\dots, N_{\mathbf{k}}, \dots\rangle &= \sqrt{N_{\mathbf{k}} + 1}|\dots, N_{\mathbf{k}}, \dots\rangle \\ \alpha_{\mathbf{k}}(\beta_{\mathbf{k}})|\dots, N_{\mathbf{k}}, \dots\rangle &= \sqrt{N_{\mathbf{k}}}|\dots, N_{\mathbf{k}}, \dots\rangle. \end{aligned}$$

Since the energies are degenerate, we omit differentiating between the two types of magnon distribution functions. After obtaining the scattering rate, we linearize it with respect to $\delta N_{\mathbf{k}}$, where $N_{\mathbf{k}} = \bar{N}_{\mathbf{k}} + \delta N_{\mathbf{k}}$, $\bar{N}_{\mathbf{k}}$ is the Bose-Einstein distribution, and $\delta N_{\mathbf{k}}$ is the out-of-equilibrium distribution. This amounts to writing

$$\Gamma_{\mathbf{k}}[\{N_{\mathbf{k}_i}\}] = \sum_{\mathbf{k}'} C_{\mathbf{k}\mathbf{k}'} \delta N_{\mathbf{k}'}, \quad (98)$$

where $C_{\mathbf{k}\mathbf{k}'}$ is a matrix containing the collision kernel. The diagonal elements of $C_{\mathbf{k}\mathbf{k}'}$ are denoted by $D_{\mathbf{k}}$, which is also the inverse relaxation time $D_{\mathbf{k}} = \tau_{\mathbf{k}}^{-1}$. One can also introduce a phenomenological damping term into $D_{\mathbf{k}}$, but we do not consider such a term here. The off-diagonal elements are denoted by $O_{\mathbf{k}\mathbf{k}'}$, and are the elements that will contribute to the thermal Hall conductivity. We switch to Hardy's basis, such that $C_{\mathbf{k}\mathbf{k}'} = \frac{G_{\mathbf{k}'}}{G_{\mathbf{k}}} C_{\mathbf{k}\mathbf{k}'}$, where $G_{\mathbf{k}} = \sqrt{\bar{N}_{\mathbf{k}}(\bar{N}_{\mathbf{k}} + 1)}$. The thermal conductivity tensor is given by

$$\kappa_{\text{th}} = -\frac{1}{k_B T^2 V} \sum_{\mathbf{k}\mathbf{k}'} \mathbf{v}_{\mathbf{k}} \otimes \mathbf{v}_{\mathbf{k}'} \varepsilon_{\mathbf{k}} \varepsilon_{\mathbf{k}'} G_{\mathbf{k}} G_{\mathbf{k}'} [\mathcal{C}^{-1}]_{\mathbf{k}\mathbf{k}'}. \quad (99)$$

After symmetrizing, the thermal Hall conductivity is given by

$$\kappa_{\text{th,H}} = \frac{1}{2k_B T^2 V} \sum_{\mathbf{k}, \mathbf{k}'} (\mathbf{v}_{\mathbf{k}} \times \mathbf{v}_{\mathbf{k}'})_z \varepsilon_{\mathbf{k}} \varepsilon_{\mathbf{k}'} \tau_{\mathbf{k}} \tau_{\mathbf{k}'} G_{\mathbf{k}} G_{\mathbf{k}'} \left(\frac{\mathcal{O}_{\mathbf{k}\mathbf{k}'} - \mathcal{O}_{\mathbf{k}'\mathbf{k}}}{2} \right), \quad (100)$$

where

$$\mathcal{O}_{\mathbf{k}\mathbf{k}'} = \mathcal{O}_{\mathbf{k}\mathbf{k}'}^{\text{in}} - \mathcal{O}_{\mathbf{k}\mathbf{k}'}^{\text{out}} = (\mathcal{O}_{\mathbf{k}\mathbf{k}'}^{++} + \mathcal{O}_{\mathbf{k}\mathbf{k}'}^{+-}) - (\mathcal{O}_{\mathbf{k}\mathbf{k}'}^{-+} + \mathcal{O}_{\mathbf{k}\mathbf{k}'}^{--}). \quad (101)$$

Then the antisymmetric part of the collision kernel is given by

$$\left(\frac{\mathcal{O}_{\mathbf{k}\mathbf{k}'} - \mathcal{O}_{\mathbf{k}'\mathbf{k}}}{2} \right) = \frac{\bar{N}_{\mathbf{k}'} - \bar{N}_{\mathbf{k}}}{2\bar{N}_{\mathbf{k}'}} (\mathcal{O}_{\mathbf{k}\mathbf{k}'}^{++} - e^{-\beta \varepsilon_{\mathbf{k}'}} \mathcal{O}_{\mathbf{k}\mathbf{k}'}^{--}) + \frac{\bar{N}_{\mathbf{k}'} + \bar{N}_{\mathbf{k}} + 1}{2\bar{N}_{\mathbf{k}'}} (e^{-\beta \varepsilon_{\mathbf{k}'}} \mathcal{O}_{\mathbf{k}\mathbf{k}'}^{+-} - \mathcal{O}_{\mathbf{k}\mathbf{k}'}^{-+}). \quad (102)$$

The key point here is that the terms that will contribute something finite to $\kappa_{\text{th,H}}$ are the terms that break the microscopic detailed-balance conditions, as mentioned in the main text.

S7.5 Scattering from interactions

We may depict the different scattering processes using Feynman diagrams. We choose the convention that an arrow going into a vertex creates a quasiparticle in the diagonal basis, and an arrow leaving a vertex annihilates one. The scattering transition probabilities $|T_{\text{if}}|^2$ result in a change in net magnon number $\Delta N = \{-4, -2, 0, 2, 4\}$.

Due to the Bogoliubov transformation, we have many vertices, thus we group them in terms of net magnon number. Each scattering channel will contribute something positive definite, thus we examine one process in the $\Delta N = 0$ channel as an example. We consider a 2-in-2-out process

$$|i\rangle = |N_{\mathbf{k}}, N_{\mathbf{k}_1}, N_{\mathbf{k}_2}, N_{\mathbf{k}_3}\rangle \quad |f\rangle = |N_{\mathbf{k}} - 1, N_{\mathbf{k}_1} - 1, N_{\mathbf{k}_2} + 1, N_{\mathbf{k}_3} + 1\rangle \quad (103)$$

so the transition probability is

$$|T_{\text{if}}|^2 = \left| T_{\text{if}}^{(1)} + T_{\text{if}}^{(2)} \right|^2 = \left| \begin{array}{c} \text{diagram 1} + \text{diagram 2} + \dots \end{array} \right|^2, \quad (104)$$

where the \dots correspond to other tree and bubble diagrams with $\Delta N = 0$.

From Fermi's golden rule, the scattering rates can be calculated with

$$\Gamma_{\text{if}}^{(1)}[\{N_{\mathbf{k}'}\}] = \frac{2\pi}{\hbar} |T_{\text{if}}^{(1)}|^2 \delta(E_f - E_i) \quad (105)$$

$$\Gamma_{\text{if}}^{(2)}[\{N_{\mathbf{k}'}\}] = \frac{2\pi}{\hbar} |T_{\text{if}}^{(2)}|^2 \delta(E_f - E_i) \quad (106)$$

$$\Gamma_{\text{if}}^{(1,2)}[\{N_{\mathbf{k}'}\}] = \frac{4\pi}{\hbar} \delta(E_f - E_i) \left[\text{Re}(T_{\text{if}}^{(1)}) \text{Re}(T_{\text{if}}^{(2)}) + \text{Im}(T_{\text{if}}^{(1)}) \text{Im}(T_{\text{if}}^{(2)}) \right]. \quad (107)$$

Note that both $\Gamma_{\text{if}}^{(1)}$ and $\Gamma_{\text{if}}^{(2)}$ are positive definite, whereas $\Gamma_{\text{if}}^{(1,2)}$ can be either positive or negative. However, since $\Gamma_{\text{if}}^{(1)} \sim O(J_{\chi}^2)$, $\Gamma_{\text{if}}^{(1,2)} \sim O(J_{\chi}^3)$, $\Gamma_{\text{if}}^{(2)} \sim O(J_{\chi}^4)$, then $\Gamma_{\text{if}}^{(1)} > \Gamma_{\text{if}}^{(1,2)} > \Gamma_{\text{if}}^{(2)}$. Thus, although $\Gamma_{\text{if}}^{(1,2)}$ can be positive or negative, the total scattering rate $\Gamma_{\text{if}} > 0$ since it will be $\Gamma_{\text{if}}^{(1)} \pm$ a small number (otherwise the perturbation theory breaks down).

S7.5.1 First order contribution

At first order in J_χ and S , the out-scattering process (2-in-2-out, denoted by +2 for 2 magnons out) is given by

$$\Gamma_{\mathbf{k}}^{(1),\text{out}} = \frac{2\pi}{\hbar} \sum_{\mathbf{k}_1, \mathbf{k}_2, \mathbf{k}_3} \delta(\varepsilon_{\mathbf{k}} + \varepsilon_{\mathbf{k}_1} - \varepsilon_{\mathbf{k}_2} - \varepsilon_{\mathbf{k}_3}) \delta_{\mathbf{k}+\mathbf{k}_1-\mathbf{k}_2-\mathbf{k}_3} |W_{\mathbf{k}, \mathbf{k}_1, \mathbf{k}_2, \mathbf{k}_3}^{+2}|^2 N_{\mathbf{k}} N_{\mathbf{k}_1} (N_{\mathbf{k}_2} + 1) (N_{\mathbf{k}_3} + 1), \quad (108)$$

and the in-scattering process (2-out-2-in, denoted by -2 for two magnons in) is given by

$$\Gamma_{\mathbf{k}}^{(1),\text{in}} = \frac{2\pi}{\hbar} \sum_{\mathbf{k}_1, \mathbf{k}_2, \mathbf{k}_3} \delta(\varepsilon_{\mathbf{k}} + \varepsilon_{\mathbf{k}_1} - \varepsilon_{\mathbf{k}_2} - \varepsilon_{\mathbf{k}_3}) \delta_{\mathbf{k}+\mathbf{k}_1-\mathbf{k}_2-\mathbf{k}_3} |W_{\mathbf{k}, \mathbf{k}_1, \mathbf{k}_2, \mathbf{k}_3}^{+2}|^2 (N_{\mathbf{k}} + 1) (N_{\mathbf{k}_1} + 1) N_{\mathbf{k}_2} N_{\mathbf{k}_3}, \quad (109)$$

where we used $W_{\mathbf{k}, \mathbf{k}_1, \mathbf{k}_2, \mathbf{k}_3}^{-2} = \left(W_{\mathbf{k}, \mathbf{k}_1, \mathbf{k}_2, \mathbf{k}_3}^{+2}\right)^*$. Next, we linearize $\Gamma_{\mathbf{k}}^{(1)} = \Gamma_{\mathbf{k}}^{(1),\text{in}} - \Gamma_{\mathbf{k}}^{(1),\text{out}}$ such that

$$\Gamma_{\mathbf{k}}^{(1)} = C [\{\bar{N}_{\mathbf{k}}, \bar{N}_{\mathbf{k}_1}, \bar{N}_{\mathbf{k}_2}, \bar{N}_{\mathbf{k}_3}\}] + D_{\mathbf{k}} \delta N_{\mathbf{k}} + \sum_{\mathbf{k}_1} O_{\mathbf{k}, \mathbf{k}_1} \delta N_{\mathbf{k}_1} + \sum_{\mathbf{k}_2} O_{\mathbf{k}, \mathbf{k}_2} \delta N_{\mathbf{k}_2} + \sum_{\mathbf{k}_3} O_{\mathbf{k}, \mathbf{k}_3} \delta N_{\mathbf{k}_3}. \quad (110)$$

Noting that $(\bar{N}_{\mathbf{k}} + 1) = e^{\beta \varepsilon_{\mathbf{k}}} \bar{N}_{\mathbf{k}}$ and using momentum conservation, the constant shift C is

$$\begin{aligned} C [\{\bar{N}_{\mathbf{k}}, \bar{N}_{\mathbf{k}_1}, \bar{N}_{\mathbf{k}_2}, \bar{N}_{\mathbf{k}_3}\}] &= \frac{2\pi}{\hbar} \sum_{\mathbf{k}_1, \mathbf{k}_2, \mathbf{k}_3} \delta(\varepsilon_{\mathbf{k}} + \varepsilon_{\mathbf{k}_1} - \varepsilon_{\mathbf{k}_2} - \varepsilon_{\mathbf{k}_3}) \delta_{\mathbf{k}+\mathbf{k}_1-\mathbf{k}_2-\mathbf{k}_3} |W_{\mathbf{k}, \mathbf{k}_1, \mathbf{k}_2, \mathbf{k}_3}^{+2}|^2 \\ &\quad \times [(\bar{N}_{\mathbf{k}} + 1)(\bar{N}_{\mathbf{k}_1} + 1)\bar{N}_{\mathbf{k}_2}\bar{N}_{\mathbf{k}_3} - \bar{N}_{\mathbf{k}}\bar{N}_{\mathbf{k}_1}(\bar{N}_{\mathbf{k}_2} + 1)(\bar{N}_{\mathbf{k}_3} + 1)] \\ &= 0. \end{aligned} \quad (111)$$

Here, C is expected to be zero since there should not be any finite current at equilibrium. The diagonal scattering rate is

$$D_{\mathbf{k}} = \frac{2\pi}{\hbar} \sum_{\mathbf{k}_1, \mathbf{k}_2, \mathbf{k}_3} \delta(\varepsilon_{\mathbf{k}} + \varepsilon_{\mathbf{k}_1} - \varepsilon_{\mathbf{k}_2} - \varepsilon_{\mathbf{k}_3}) \delta_{\mathbf{k}+\mathbf{k}_1-\mathbf{k}_2-\mathbf{k}_3} |W_{\mathbf{k}, \mathbf{k}_1, \mathbf{k}_2, \mathbf{k}_3}^{+2}|^2 \frac{(\bar{N}_{\mathbf{k}_1} + 1)\bar{N}_{\mathbf{k}_2}\bar{N}_{\mathbf{k}_3}}{\bar{N}_{\mathbf{k}}} \quad (112)$$

and the off-diagonal elements are

$$O_{\mathbf{k}, \mathbf{k}_1} = \frac{2\pi}{\hbar} \sum_{\mathbf{k}_2, \mathbf{k}_3} \delta(\varepsilon_{\mathbf{k}} + \varepsilon_{\mathbf{k}_1} - \varepsilon_{\mathbf{k}_2} - \varepsilon_{\mathbf{k}_3}) \delta_{\mathbf{k}+\mathbf{k}_1-\mathbf{k}_2-\mathbf{k}_3} |W_{\mathbf{k}, \mathbf{k}_1, \mathbf{k}_2, \mathbf{k}_3}^{+2}|^2 \frac{(\bar{N}_{\mathbf{k}} + 1)\bar{N}_{\mathbf{k}_2}\bar{N}_{\mathbf{k}_3}}{\bar{N}_{\mathbf{k}_1}} \quad (113)$$

$$O_{\mathbf{k}, \mathbf{k}_2} = \frac{2\pi}{\hbar} \sum_{\mathbf{k}_1, \mathbf{k}_3} \delta(\varepsilon_{\mathbf{k}} + \varepsilon_{\mathbf{k}_1} - \varepsilon_{\mathbf{k}_2} - \varepsilon_{\mathbf{k}_3}) \delta_{\mathbf{k}+\mathbf{k}_1-\mathbf{k}_2-\mathbf{k}_3} |W_{\mathbf{k}, \mathbf{k}_1, \mathbf{k}_2, \mathbf{k}_3}^{+2}|^2 \frac{(\bar{N}_{\mathbf{k}} + 1)(\bar{N}_{\mathbf{k}_1} + 1)\bar{N}_{\mathbf{k}_3}}{\bar{N}_{\mathbf{k}_2}} \quad (114)$$

$$O_{\mathbf{k}, \mathbf{k}_3} = \frac{2\pi}{\hbar} \sum_{\mathbf{k}_1, \mathbf{k}_2} \delta(\varepsilon_{\mathbf{k}} + \varepsilon_{\mathbf{k}_1} - \varepsilon_{\mathbf{k}_2} - \varepsilon_{\mathbf{k}_3}) \delta_{\mathbf{k}+\mathbf{k}_1-\mathbf{k}_2-\mathbf{k}_3} |W_{\mathbf{k}, \mathbf{k}_1, \mathbf{k}_2, \mathbf{k}_3}^{+2}|^2 \frac{(\bar{N}_{\mathbf{k}} + 1)(\bar{N}_{\mathbf{k}_1} + 1)\bar{N}_{\mathbf{k}_2}}{\bar{N}_{\mathbf{k}_3}}. \quad (115)$$

To examine if the off-diagonal components contribute to $\kappa_{\text{th}, \text{H}}$, we rewrite $O_{\mathbf{k}, \mathbf{k}'}$ in Hardy's basis:

$$\mathcal{O}_{\mathbf{k}, \mathbf{k}'} = \frac{\sqrt{(\bar{N}_{\mathbf{k}'} + 1) \bar{N}_{\mathbf{k}'}}}{\sqrt{(\bar{N}_{\mathbf{k}} + 1) \bar{N}_{\mathbf{k}}}} O_{\mathbf{k}, \mathbf{k}'}. \quad (116)$$

As an example, we examine $\mathcal{O}_{\mathbf{k}, \mathbf{k}_1}$ in Hardy's basis, given by

$$\mathcal{O}_{\mathbf{k}, \mathbf{k}_1} = \frac{2\pi}{\hbar} \sum_{\mathbf{k}_2, \mathbf{k}_3} \delta(\varepsilon_{\mathbf{k}} + \varepsilon_{\mathbf{k}_1} - \varepsilon_{\mathbf{k}_2} - \varepsilon_{\mathbf{k}_3}) \delta_{\mathbf{k}+\mathbf{k}_1-\mathbf{k}_2-\mathbf{k}_3} |W_{\mathbf{k}, \mathbf{k}_1, \mathbf{k}_2, \mathbf{k}_3}^{+2}|^2 \frac{\sqrt{(\bar{N}_{\mathbf{k}_1} + 1) (\bar{N}_{\mathbf{k}} + 1)}}{\sqrt{\bar{N}_{\mathbf{k}} \bar{N}_{\mathbf{k}_1}}} \bar{N}_{\mathbf{k}_2} \bar{N}_{\mathbf{k}_3}. \quad (117)$$

Since \mathbf{k} and \mathbf{k}_1 play the same role, swapping these will not change the vertex. Thus, it is clear that $\mathcal{O}_{\mathbf{k}, \mathbf{k}_1} - \mathcal{O}_{\mathbf{k}_1, \mathbf{k}} = 0$, implying it doesn't contribute to $\kappa_{\text{th}, \text{H}}$. A similar argument can be made for $\mathcal{O}_{\mathbf{k}, \mathbf{k}_2}$ and $\mathcal{O}_{\mathbf{k}, \mathbf{k}_3}$, thus the first order diagrams in $\Delta N = 0$ cannot generate a finite thermal Hall effect. Indeed, it was shown that all first order off-diagonal scattering processes for magnons [17] as well as phonons [18] do not contribute to transverse thermal transport.

S7.5.2 Interference term

As an example, we examine the interference between the tree level diagram and the bubble composed of 1-out-3-in (-3) and 1-in 3-out (+3) processes with $\Delta N = 0$. We have

$$T_{\text{if}}^{(1),\text{out}} = W_{\mathbf{k}\mathbf{k}_1\mathbf{k}_2\mathbf{k}_3}^{+2} \sqrt{N_{\mathbf{k}}N_{\mathbf{k}_1}(N_{\mathbf{k}_2}+1)(N_{\mathbf{k}_3}+1)} \delta_{\mathbf{k}+\mathbf{k}_1-\mathbf{k}_2-\mathbf{k}_3} \quad (118)$$

and

$$T_{\text{if}}^{(2),\text{out}} = \sqrt{N_{\mathbf{k}}N_{\mathbf{k}_1}(N_{\mathbf{k}_2}+1)(N_{\mathbf{k}_3}+1)} \times \sum_{\mathbf{p}_1\mathbf{p}_2} \frac{W_{\mathbf{k}_1\mathbf{p}_1\mathbf{p}_2\mathbf{k}}^{-3} W_{\mathbf{k}_2\mathbf{p}_2\mathbf{p}_1\mathbf{k}_3}^{+3} (N_{\mathbf{p}_1}+1) N_{\mathbf{p}_2}}{\varepsilon_{\mathbf{k}_1} + \varepsilon_{\mathbf{k}} - \varepsilon_{\mathbf{p}_1} + \varepsilon_{\mathbf{p}_2} + i\eta} \delta_{\mathbf{k}+\mathbf{k}_1+\mathbf{p}_2,\mathbf{p}_1} \delta_{\mathbf{p}_2+\mathbf{k}_2+\mathbf{k}_3,\mathbf{p}_1}. \quad (119)$$

Let $\Delta E = \varepsilon_{\mathbf{k}_1} + \varepsilon_{\mathbf{k}} - \varepsilon_{\mathbf{p}_1} + \varepsilon_{\mathbf{p}_2}$. The real and imaginary parts of $T_{\text{if}}^{(2),\text{out}}$ can be obtained using $\frac{1}{\Delta E + i\eta} = \mathcal{P}\left(\frac{1}{\Delta E}\right) - i\pi\delta(\Delta E)$. Putting everything together, the total scattering rate for the 2-in-2-out tree \times 3-in 1-out / 1-in 3-out bubble is

$$\Gamma_{\mathbf{k}}^{(1,2),\text{out}} = \frac{4\pi}{\hbar} \frac{1}{2} \sum_{\mathbf{k}_1\mathbf{k}_2\mathbf{k}_3} N_{\mathbf{k}}N_{\mathbf{k}_1}(N_{\mathbf{k}_2}+1)(N_{\mathbf{k}_3}+1) \delta_{\mathbf{k}+\mathbf{k}_1-\mathbf{k}_2-\mathbf{k}_3} \delta(\varepsilon_{\mathbf{k}} + \varepsilon_{\mathbf{k}_1} - \varepsilon_{\mathbf{k}_2} - \varepsilon_{\mathbf{k}_3}) \times \sum_{\mathbf{p}_1\mathbf{p}_2} (N_{\mathbf{p}_1}+1) N_{\mathbf{p}_2} \delta_{\mathbf{k}+\mathbf{k}_1+\mathbf{p}_2,\mathbf{p}_1} \delta_{\mathbf{p}_2+\mathbf{k}_2+\mathbf{k}_3,\mathbf{p}_1} [\mathcal{R}_{\text{S}}^{\text{out}} + \mathcal{R}_{\text{AS}}^{\text{out}}], \quad (120)$$

where the extra factor of 1/2 comes from separating the expression into its symmetric and antisymmetric components

$$\begin{aligned} \mathcal{R}_{\text{S}}^{\text{out}} &= \mathcal{P}\left(\frac{1}{\Delta E}\right) [\text{Re}(W_{+2})A + \text{Im}(W_{+2})B] + \pi\delta(\Delta E) [\text{Re}(W_{+2})B - \text{Im}(W_{+2})A] \text{ and} \\ \mathcal{R}_{\text{AS}}^{\text{out}} &= \mathcal{P}\left(\frac{1}{\Delta E}\right) [\text{Re}(W_{+2})A - \text{Im}(W_{+2})B] + \pi\delta(\Delta E) [\text{Re}(W_{+2})B + \text{Im}(W_{+2})A]. \end{aligned} \quad (121)$$

For brevity, in the above we have denoted $W_{\mathbf{k}\mathbf{k}_1\mathbf{k}_2\mathbf{k}_3}^{+2} \equiv W_{+2}$, $W_{\mathbf{k}_1\mathbf{p}_1\mathbf{p}_2\mathbf{k}}^{-3} \equiv W_{-3}$, and $W_{\mathbf{k}_2\mathbf{p}_2\mathbf{p}_1\mathbf{k}_3}^{+3} \equiv W_{+3}$.

Similarly, the scattering rate for the in-process is given by

$$\begin{aligned} \Gamma_{\mathbf{k}}^{(1,2),\text{in}} &= \frac{4\pi}{\hbar} \frac{1}{2} \sum_{\mathbf{k}_1\mathbf{k}_2\mathbf{k}_3} (N_{\mathbf{k}}+1)(N_{\mathbf{k}_1}+1)N_{\mathbf{k}_2}N_{\mathbf{k}_3} \delta(\varepsilon_{\mathbf{k}} + \varepsilon_{\mathbf{k}_1} - \varepsilon_{\mathbf{k}_2} - \varepsilon_{\mathbf{k}_3}) \delta_{\mathbf{k}+\mathbf{k}_1-\mathbf{k}_2-\mathbf{k}_3} \times \\ &\sum_{\mathbf{p}_1\mathbf{p}_2} N_{\mathbf{p}_2} (N_{\mathbf{p}_1}+1) \delta_{\mathbf{k}+\mathbf{k}_1+\mathbf{p}_2,\mathbf{p}_1} \delta_{\mathbf{p}_2+\mathbf{k}_2+\mathbf{k}_3,\mathbf{p}_1} [\mathcal{R}_{\text{S}}^{\text{in}} + \mathcal{R}_{\text{AS}}^{\text{in}}], \end{aligned} \quad (122)$$

where $\mathcal{R}_{\text{S}}^{\text{in}} = (\mathcal{R}_{\text{S}}^{\text{out}})^*$ and $\mathcal{R}_{\text{AS}}^{\text{in}} = (\mathcal{R}_{\text{AS}}^{\text{out}})^*$. Next, we perform the same procedure of linearizing and transforming into Hardy's basis. In this case, the off-diagonal components always correspond to $\mathcal{O}_{\mathbf{k}\mathbf{k}'}^{++}$ or $\mathcal{O}_{\mathbf{k}\mathbf{k}'}^{--}$ type processes, so the terms contributing to $\kappa_{\text{th,H}}$ will be those who break $\mathcal{O}_{\mathbf{k}\mathbf{k}'}^{++}/\mathcal{O}_{\mathbf{k}\mathbf{k}'}^{--} = e^{-\beta\varepsilon_{\mathbf{k}'}}$. Using the fact that $\text{Im}(W) = -\text{Im}(W^*)$, and that $(\bar{N}_{\mathbf{k}}+1) = e^{\beta\varepsilon_{\mathbf{k}}}\bar{N}_{\mathbf{k}}$, we have

$$\begin{aligned} \mathcal{O}_{\mathbf{k}\mathbf{k}_1}^{++} &= \frac{4\pi^2}{\hbar} \frac{1}{2} \sum_{\mathbf{k}_2\mathbf{k}_3} \delta(\varepsilon_{\mathbf{k}} + \varepsilon_{\mathbf{k}_1} - \varepsilon_{\mathbf{k}_2} - \varepsilon_{\mathbf{k}_3}) \delta_{\mathbf{k}+\mathbf{k}_1-\mathbf{k}_2-\mathbf{k}_3} \bar{N}_{\mathbf{k}_1} \bar{N}_{\mathbf{k}_2} \bar{N}_{\mathbf{k}_3} \sqrt{e^{\beta(\varepsilon_{\mathbf{k}_1}+\varepsilon_{\mathbf{k}})}} \\ &\times \sum_{\mathbf{p}_1\mathbf{p}_2} (\bar{N}_{\mathbf{p}_1}+1) \bar{N}_{\mathbf{p}_2} \delta_{\mathbf{k}+\mathbf{k}_1+\mathbf{p}_2,\mathbf{p}_1} \delta_{\mathbf{p}_2+\mathbf{k}_2+\mathbf{k}_3,\mathbf{p}_1} \delta(\varepsilon_{\mathbf{k}_1} + \varepsilon_{\mathbf{k}} - \varepsilon_{\mathbf{p}_1} + \varepsilon_{\mathbf{p}_2}) \\ &\times (-\text{Im}(W_{+2}) [\text{Re}(W_{+3})\text{Re}(W_{-3}) - \text{Im}(W_{+3})\text{Im}(W_{-3})] \\ &- \text{Re}(W_{+2}) [\text{Re}(W_{+3})\text{Im}(W_{-3}) - \text{Im}(W_{+3})\text{Re}(W_{-3})]) \end{aligned} \quad (123)$$

$$= -e^{-\beta\varepsilon_{\mathbf{k}_1}} \mathcal{O}_{\mathbf{k}\mathbf{k}_1}^{--} \quad (124)$$

which obeys anti-detailed balance. A similar situation arises for $\mathcal{O}_{\mathbf{k}\mathbf{k}_2}$ and $\mathcal{O}_{\mathbf{k}\mathbf{k}_3}$. Thus, the thermal Hall conductivity is given by

$$\begin{aligned} \kappa_{\text{th,H}} &= \frac{1}{4k_B T^2 V} \sum_{\mathbf{k},\mathbf{k}'} \mathbf{v}_{\mathbf{k}} \times \mathbf{v}_{\mathbf{k}'} \varepsilon_{\mathbf{k}} \varepsilon_{\mathbf{k}'} \tau_{\mathbf{k}} \tau_{\mathbf{k}'} G_{\mathbf{k}} G_{\mathbf{k}'} \frac{\bar{N}_{\mathbf{k}'} - \bar{N}_{\mathbf{k}}}{\bar{N}_{\mathbf{k}'}} (\mathcal{O}_{\mathbf{k}\mathbf{k}'}^{++} - e^{-\beta\varepsilon_{\mathbf{k}'}} \mathcal{O}_{\mathbf{k}\mathbf{k}'}^{--}) \\ &= \frac{1}{2k_B T^2 V} \sum_{\mathbf{k},\mathbf{k}'} \mathbf{v}_{\mathbf{k}} \times \mathbf{v}_{\mathbf{k}'} \varepsilon_{\mathbf{k}} \varepsilon_{\mathbf{k}'} \tau_{\mathbf{k}} \tau_{\mathbf{k}'} G_{\mathbf{k}} G_{\mathbf{k}'} \frac{\bar{N}_{\mathbf{k}'} - \bar{N}_{\mathbf{k}}}{\bar{N}_{\mathbf{k}'}} \mathcal{O}_{\mathbf{k}\mathbf{k}'}^{++}. \end{aligned}$$

From Eq. 123, it is clear that only odd powers of J_χ may contribute something finite to $\kappa_{\text{th,H}}$, since the vertices from J_1 and J_2 are purely real, while those from J_χ are purely imaginary. To the lowest order of J_χ , $\kappa_{\text{th,H}} \propto J_1^2 J_\chi / S^2 \propto \sin(\pi\Phi/\Phi_0)$. In this case, the behaviour of $\kappa_{\text{th,H}}$ reflects the fact that the J_χ interaction in the Hamiltonian is TR odd.

S8 Supplemental Plots

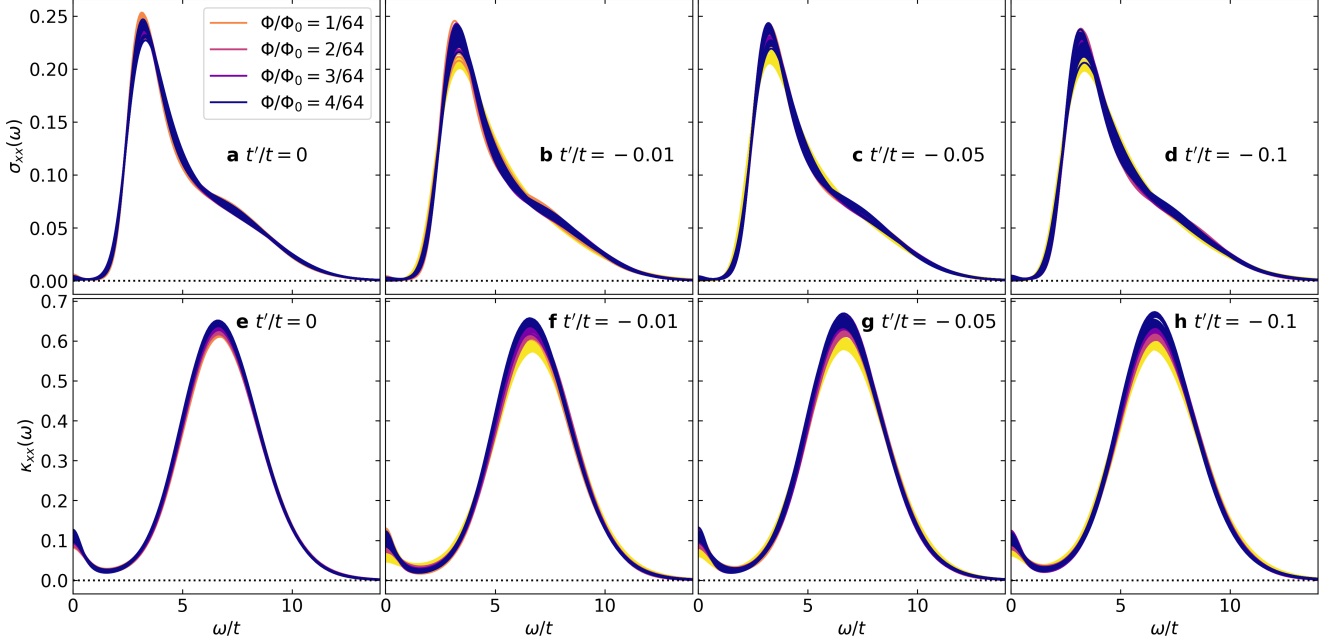


Figure S6: Example of minimal magnetic field strength and t'/t dependence of longitudinal optical conductivity $\sigma_{xx}(\omega)$ and longitudinal frequency-dependent thermal conductivity $\kappa_{xx}(\omega)$. Temperature $\beta t = 5$, Hubbard $U/t = 6$. All panels share the same legend.

References

- [1] Dominic Bergeron and A.-M. S. Tremblay. Algorithms for optimized maximum entropy and diagnostic tools for analytic continuation. *Phys. Rev. E*, 94:023303, Aug 2016.
- [2] G.D. Mahan. *Many-Particle Physics*. Physics of Solids and Liquids. Springer US, 2013.
- [3] M.P. Marder. *Condensed Matter Physics*. Wiley, 2010.
- [4] B. Sriram Shastry. Electrothermal transport coefficients at finite frequencies. *Reports on Progress in Physics*, 72(1):016501, December 2008.
- [5] J. M. Luttinger. Theory of Thermal Transport Coefficients. *Physical Review*, 135(6A):A1505–A1514, September 1964.
- [6] Marcos Rigol and B. Sriram Shastry. Drude weight in systems with open boundary conditions. *Physical Review B*, 77(16):161101, April 2008.
- [7] Mark Jarrell and J.E. Gubernatis. Bayesian inference and the analytic continuation of imaginary-time quantum Monte Carlo data. *Physics Reports*, 269(3):133–195, 1996.
- [8] Wen O. Wang, Jixun K. Ding, Brian Moritz, Edwin W. Huang, and Thomas P. Devereaux. Magnon heat transport in a two-dimensional Mott insulator. *Phys. Rev. B*, 105:L161103, Apr 2022.

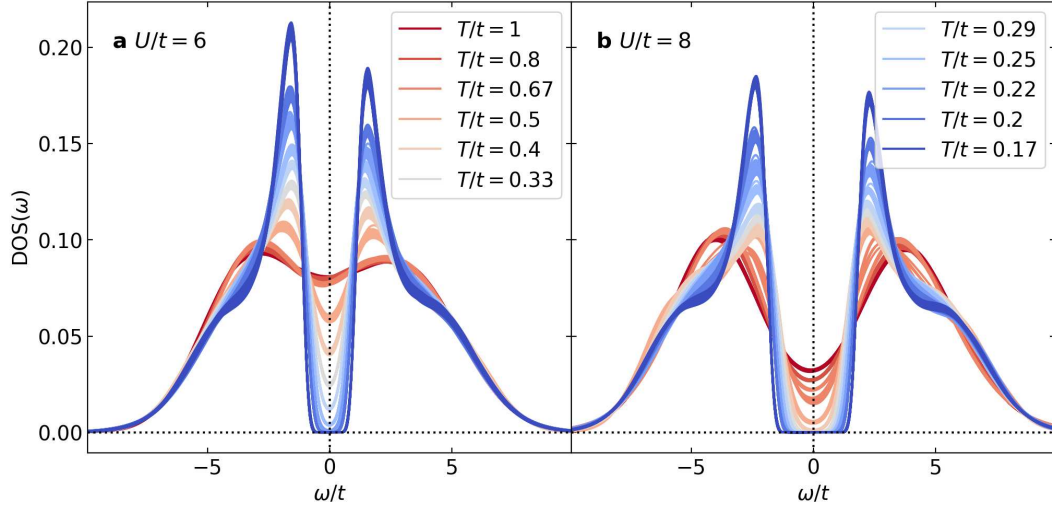


Figure S7: Temperature and Hubbard U dependence of density of states at **a** $U/t = 6$ and **b** $U/t = 8$ for the Hubbard-Hofstadter model with $t'/t = -0.1$ and fixed field strength $\Phi/\Phi_0 = 1/64$ at half filling $\langle n \rangle = 1$. 100 bootstrap resamples are shown. Both panels share the same legend.

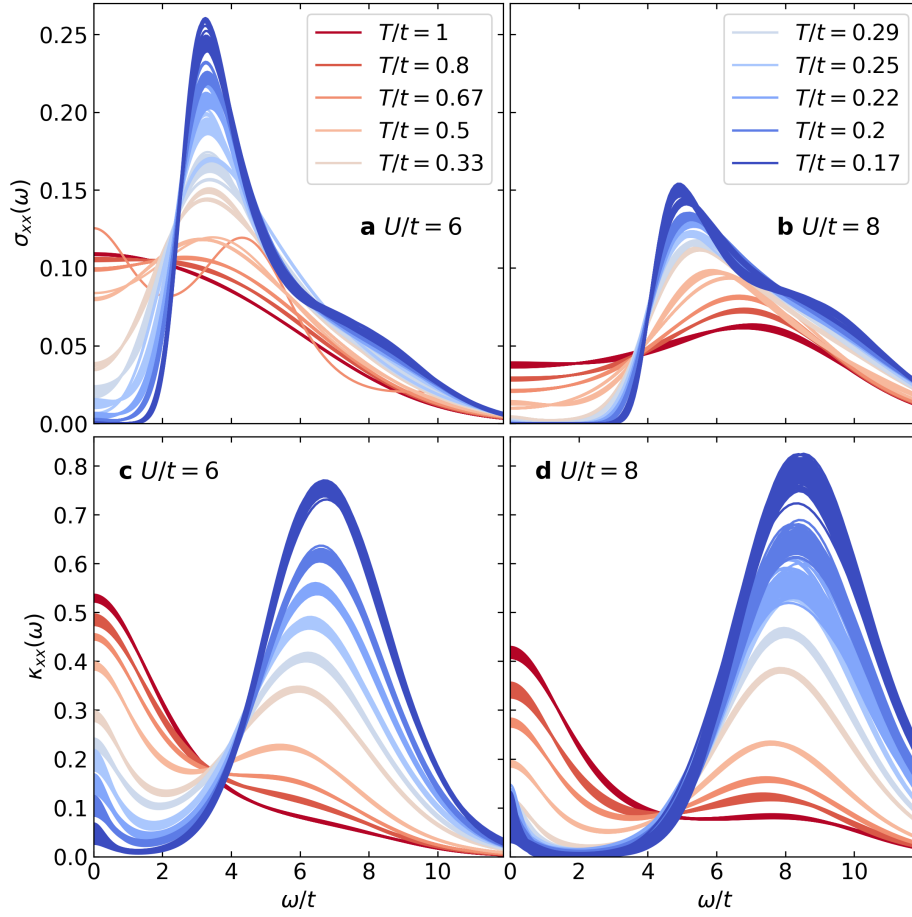


Figure S8: Temperature and Hubbard U dependence of longitudinal frequency-dependent **a c** electrical conductivity $\sigma_{xx}(\omega)$, and **b d** thermal conductivity $\kappa_{xx}(\omega)$, for the Hubbard-Hofstadter model with $t'/t = -0.1$ at half-filling $\langle n \rangle = 1$ and fixed field strength $\Phi/\Phi_0 = 1/64$. 100 bootstrap resamples are shown. All panels share the same legend.

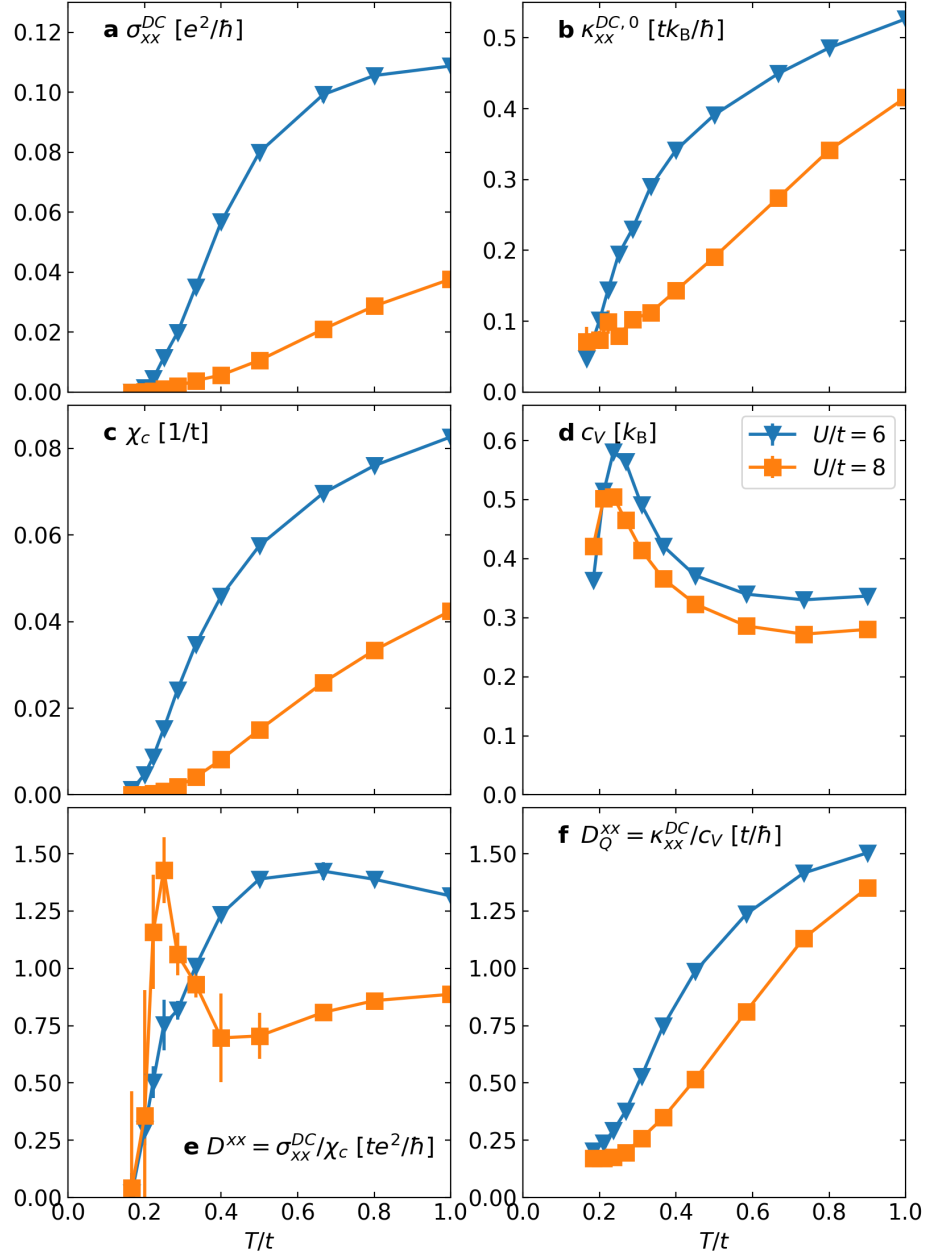


Figure S9: **a** Longitudinal DC electrical conductivity σ_{xx}^{DC} , **b** longitudinal DC thermal conductivity κ_{xx}^{DC} , **c** charge compressibility χ_c , **d** specific heat c_V , **e** charge diffusivity D^{xx} , and **f** thermal diffusivity D_Q^{xx} in the Hubbard-Hofstadter model with $t'/t = -0.1$ at half-filling $\langle n \rangle = 1$ and magnetic field strength $\Phi/\Phi_0 = 1/64$. All panels share the same legend.

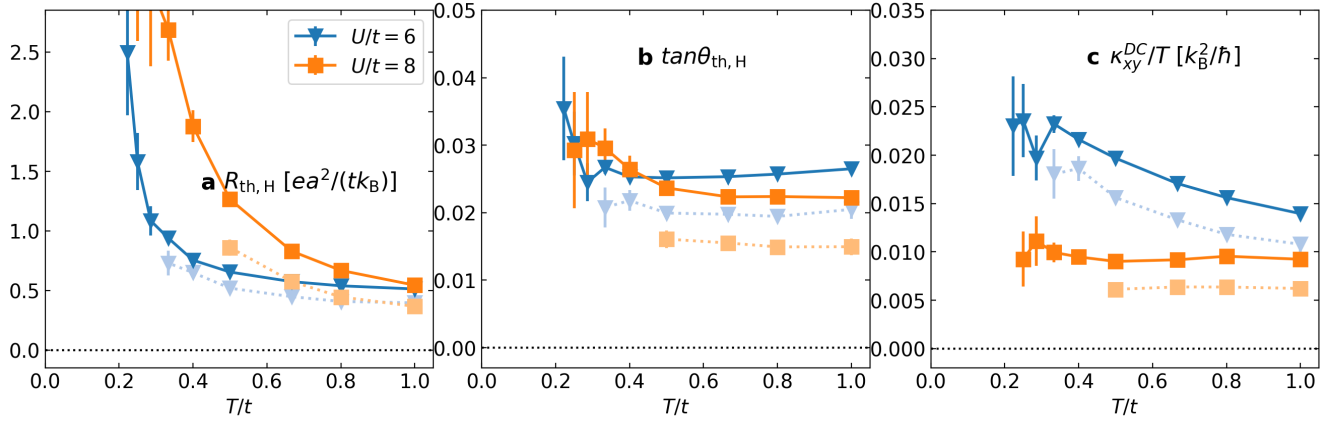


Figure S10: **a** DC thermal Hall coefficient, **b** thermal Hall angle, and **c** thermal Hall conductivity for Hubbard $U/t = 6$ and $U/t = 8$. Solid lines denote results obtained by the proxy method, while dotted lines denote results obtained by the subtraction method. Next-nearest neighbor hopping $t'/t = -0.1$ and field strength $\Phi/\Phi_0 = 1/64$. All panels share the same legend.

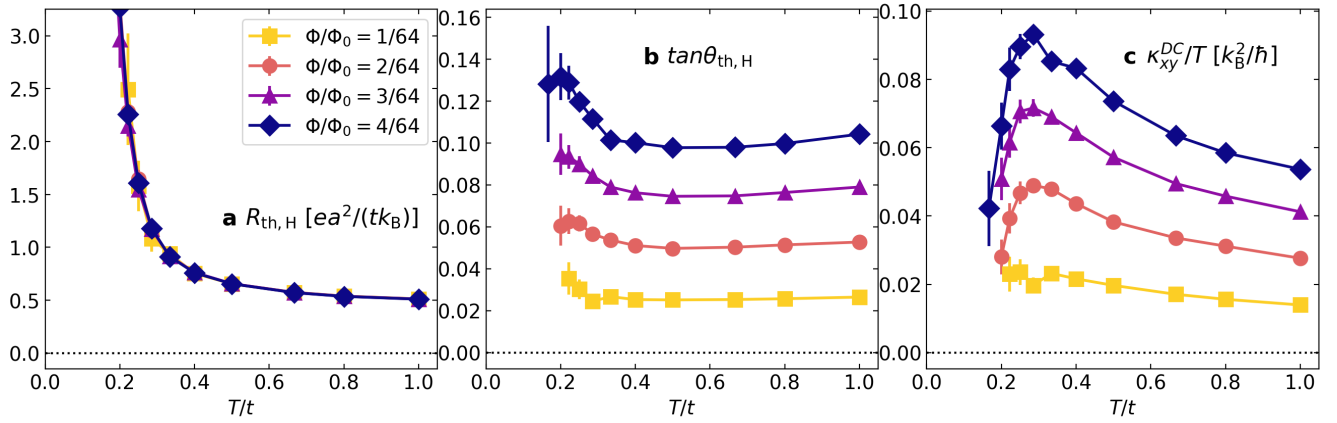


Figure S11: Magnetic field dependence of **a** DC thermal Hall coefficient, **b** thermal Hall angle, and **c** thermal Hall conductivity. Results are obtained by the proxy method. Next-nearest neighbor hopping $t'/t = -0.1$, Hubbard interaction strength U/t . All panels share the same legend.

- [9] A. Reymbaut, D. Bergeron, and A.-M. S. Tremblay. Maximum Entropy Analytic Continuation for Spectral Functions with Non-Positive Spectral Weight. *Physical Review B*, 92(6):060509, August 2015.
- [10] A. Reymbaut, A.-M. Gagnon, D. Bergeron, and A.-M. S. Tremblay. Maximum entropy analytic continuation for frequency-dependent transport coefficients with nonpositive spectral weight. *Physical Review B*, 95(12):121104, March 2017.
- [11] Wen O. Wang, Jixun K. Ding, Brian Moritz, Yoni Schattner, Edwin W. Huang, and Thomas P. Devereaux. Numerical approaches for calculating the low-field DC Hall coefficient of the doped Hubbard model. *Phys. Rev. Research*, 3:033033, Jul 2021.
- [12] F. F. Assaad and M. Imada. Hall coefficient for the two-dimensional Hubbard model. *Physical Review Letters*, 74(19):3868–3871, May 1995.
- [13] Tao Qin, Qian Niu, and Junren Shi. Energy magnetization and the thermal Hall effect. *Physical Review Letters*, 107(23):236601, November 2011.
- [14] Jung Hoon Han and Hyunyong Lee. Spin chirality and Hall-like transport phenomena of spin excitations. *Journal of the Physical Society of Japan*, 86(1):011007, January 2017.
- [15] Herbert B. Callen. The Application of Onsager’s Reciprocal Relations to Thermoelectric, Thermomagnetic, and Galvanomagnetic Effects. *Physical Review*, 73(11):1349–1358, June 1948.
- [16] Hosho Katsura, Naoto Nagaosa, and Patrick A. Lee. Theory of the thermal Hall effect in quantum magnets. *Phys. Rev. Lett.*, 104:066403, Feb 2010.
- [17] Dimos Chatzichrysafis and Alexander Mook. Thermal Hall Effect of Magnons from Many-Body Skew Scattering, June 2024.
- [18] Léo Mangeolle, Leon Balents, and Lucile Savary. Thermal conductivity and theory of inelastic scattering of phonons by collective fluctuations. *Phys. Rev. B*, 106:245139, Dec 2022.